UNIVERSITÀ
DI TORINO

Department of Oncology

PhD program: Complex Systems for Life Sciences

XXXV cycle

Identification of novel determinants of metabolic reprogramming in breast cancer

Candidate: Martino Flavia

Tutors:

Letizia Lanzetti

Federico Bussolino

Coordinator: Enzo Medico

Academic year: 2019/2023

Index

1. Abstract

Molecular signatures categorize breast tumors in four classes: Luminal A and B, HER2+ and Basal-like/Triple negative (TNBC). Among them, TNBC represents a highly heterogeneous group of tumors that lack specific markers but share a common feature: the elevated glycolytic metabolism. This project focuses on the identification of proteins that are altered in breast cancer and participate to the metabolic plasticity of these tumors. To this end, we selected a family of proteins that controls intracellular trafficking, the RabGAP proteins, based on evidence showing that membrane trafficking controls a wide number of cell properties, including cell metabolism. To identify novel glycolysis modifiers within the RabGAP family, we performed screenings by individually knocking down each of the 45 RabGAP members in TNBC cells measuring the concentration of intracellular lactate as readout of glycolysis. We crossed these results with the analysis of the correlation between gene expression and patient survival done in the METBRIC dataset. Four RabGAP proteins were found to be altered in breast cancer patients correlating with worse prognosis and all of them were shown to be required for the elevation of glycolysis in breast cancer cells. Among them, we selected TBC1D22B, a RabGAP of unknown function that localizes to the Golgi, for further studies. The function of TBC1D22B in energy metabolism has been addressed using the Seahorse technology finding that it is required for glycolysis and mitochondrial respiration. Moreover, TBC1D22B has been found to participates to lipid storage in a GAP-dependent manner. To gain insights into the molecular mechanism, we identified its protein interacting network using the proximity biotinylation technique which revealed that that the TBC1D22B interactome is mostly composed by molecules involved in cell adhesion and membrane trafficking. By employing the RUSH system, TBC1D22B was found to impair ER to Golgi transport likely by inhibiting a putative RAB target: RAB1B.

2. Introduction

2.1. Breast cancer classification

Breast cancer is a highly heterogeneous disease. Histological analysis and molecular characterization allow to classify breast tumors into four distinct subtypes based on the presence or absence of specific markers:

1) The Luminal A tumors, which express the hormone receptors estrogen and/or progesterone (ER+/PR+) and have a low percentage of proliferating cells (Ki-67< 14%);

2) The Luminal B tumors, which express the hormone receptors (ER+/PR+) and may carry amplification or overexpression of the receptor tyrosine kinase HER2 (HER2+). They have a higher number of proliferating cells compared to the Luminal A subtype as judged by a Ki-67 value greater than 14%;

3) The HER2+ tumors, they do not express the hormone receptors (ER-/PR) and carry amplification/overexpression of the receptor tyrosine kinase HER2;

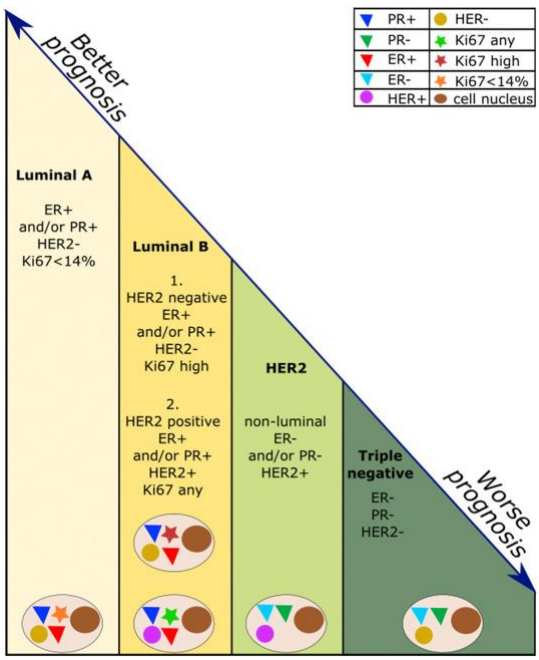

4) Basal-like breast cancers, these are tumors that express genes usually found in basal or myoepithelial cells of normal breast. This subtype includes the Triple Negative breast cancers (TNBCs) which lack all the three markers used for the classification: TNBCs are oestrogen and progesterone receptor negative (ER-), (PR-) and do not overexpress HER2 [1], [2].

Figure A: Breast cancer classification based on hormone receptor expression and the amount of cellular proliferation marker Ki67. Better or worse prognosis is directly correlated to each subtype [3]

The recognized molecular heterogeneity of breast cancer translates into different disease course, therapeutic outcome and poses important questions in patients' management. Indeed, the therapeutic approaches differ according to cancer subtype classification. Luminal A tumors tend to have lower grade compared to the other classes and are generally characterized by a more favorable prognosis. Since they express the hormone receptors, they benefit from endocrine therapy. Instead, Luminal B tumors display higher proliferation rate and are treated with a combination of chemotherapy and endocrine therapy. The HER2 overexpressing tumors are more aggressive compared to the Luminal because this subtype includes grade III tumors with higher risk of relapse. However, they can take advantage from therapeutic anti-HER2 monoclonal antibodies [1].

Finally, the most difficult to cure subtype is the TNBC. These tumors are highly aggressive, they are generally of greater size, higher grade and display lymph node involvement at diagnosis [2]. Although pre-surgical chemotherapy results in high rates of clinical response, the majority of TNBC patients suffer from distant recurrence after surgery and poorer prognosis compared to other breast cancer patients. Only 30% of patients with metastatic TNBC survive 5 years, despite adjuvant chemotherapy, which is the mainstay of treatment [1], [2], [4]. A major limitation in designing effective treatments for this group of breast cancers resides on their extreme heterogeneity and lack of markers. Identification of well-defined molecular targets to stratify patients and predict response is a currently unmet need in the TNBC patient population. In the attempt to provide targets eligible to therapeutic treatment, extensive gene expression profiling has been performed in TNBCs. This has led to the identification of seven subclasses: basal-like 1 (BL1); basal-like 2 (BL2); immunomodulatory (IM); mesenchymal (M); mesenchymal stem–like (MSL); luminal androgen receptor (LAR) and unstable (UNS) [5] that were subsequently reduced to: BL1, BL2, LAR and mesenchymal [6]. Recently, application of the immune checkpoint therapy to the TNBCs has raised consideration. However, criteria based on the analysis of the immune infiltrate to identify patients

eligible for this type of treatment have not yet reached a consensus [7]. Currently, in the clinical practice, strategies to achieve patients' stratification for prognostic judgment and therapy assignments rely on the combined evaluation of clinical and pathological parameters, which more recently have been integrated by molecular signatures of aggressive disease that provide information on the risk of relapse [8]. Furthermore, the advent of new technologies allows for the acquisition of detailed information including genomic, transcriptional and epigenetic data. During the years, platforms have been generated that correlate gene expression data, gene copy number and mutational status of the tumors with the clinical pathological parameters of the patient (https://www.cbioportal.org). Among the public available breast cancer datasets, the METABRIC (Molecular Taxonomy of Breast Cancer International Consortium) [9] and The Cancer Genome Atlas Network (TCGA) [10] are widely employed to evaluate the prognostic value of genes in breast cancer patients.

2.2 Metabolic plasticity of breast cancer

Despite the great heterogeneity that characterizes mammary tumors, there is a functional aspect shared by the more aggressive form of breast cancer correlating with prognosis: the reprogramming of cancer cells metabolism, in particular the elevation of glycolysis and the lipid consumption [11]–[15]. Breast cancer cells have been found to depend on glycolysis elevation for growth and survival [11]–[13]. Increased glycolysis generates metabolites that can be used as building blocks by other metabolic routes to synthetize nucleotide, amino acids and fatty acids required by the rapidly dividing cells to generate the tumor mass [16]. One important aspect of glycolysis elevation is the increased production of lactate by cancer cells. Lactate is produced by the enzymes L-lactate dehydrogenase (LDH) through reduction of the end-product of glycolysis, pyruvate, to L-lactic acid [17]. At physiological pH, L-lactic acid dissociates to L-lactate and proton H+ which

are then co-transported out of the cell by monocarboxylate facilitative transporters (MCT) [18].

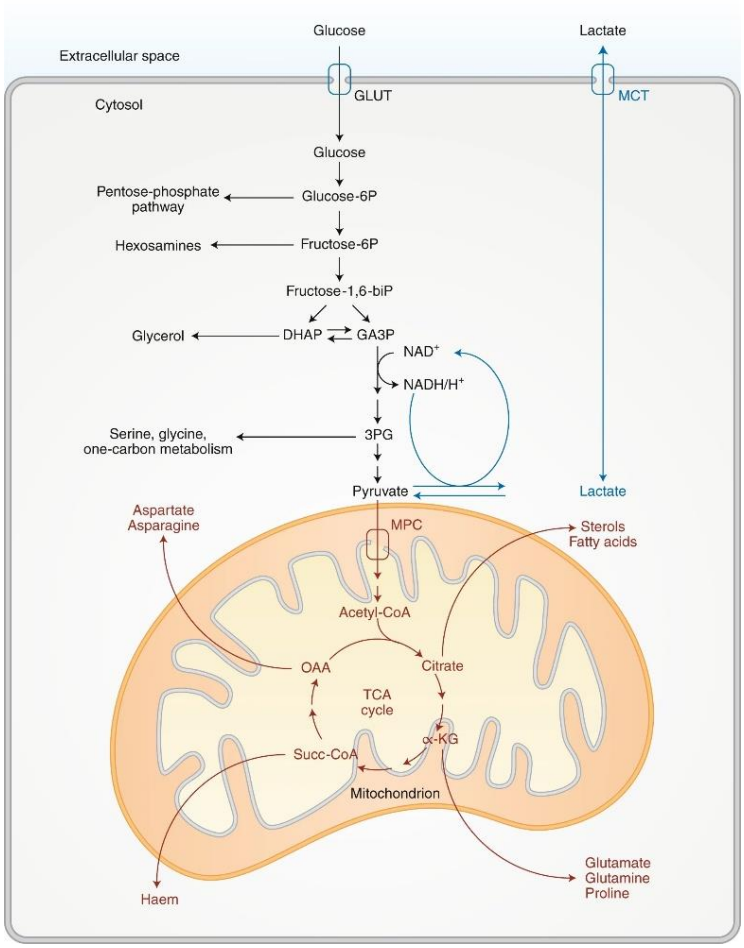

Under physiological conditions the concentration of lactate is 1.5–3mM, but in tumors it can reach up to 10–30 mM. This is due to several mechanisms that elevate glycolysis in cancer cells including also alteration and overexpression of LDH [17].

Figure B: Glycolysis and TCA-cycle are shown in black and red respectively. The lactate production as final results in glycolysis during the Warburg effect (in presence of oxygen) is highleted in blue. This step enables the recycling of NADH to NAD+ upon lactatte release [16]

Among the mechanisms responsible for the increase of glycolysis in breast cancer cells, activation of oncogenes or inhibition of oncosuppressive pathway, including the EGFR/PI3K axis, p53, MYC, and mTOR have a major role [19]. In addition, establishment of hypoxic conditions in the tumor increases the production of reactive oxygen species (ROS) inducing the expression of hypoxia inducible factor 1 (HIF-1), which boosts glucose metabolism to maintain the redox homeostasis [20]. Beside the elevation of glycolysis, major metabolic alterations, which correlate with tumor subtype, are the increased utilization of the amino acid glutamine, and the increased production (the so called *de novo* lipogenesis) and consumption

of fatty acid. Even if, intra-subtype heterogeneity has been observed, in general, TNBC tumors appear to depend more on glycolysis and on glutamine supply, while HER2+ cancers display higher glutamine metabolic activity and higher lipid metabolism compared to other subtypes [19].

Glutamine exerts several key functions in cell metabolism: i) it is a primary fuel for mammary epithelial cells which convert it to glutamate through glutaminolysis in mitochondria; ii) it provides intermediates for the biosynthesis of amino acids and nucleotides and can be exchanged with other amino acids by antiporters, iii) it counteracts oxidative stress by providing cells with glutathione and NADPH [21]. Glutamine-derived glutamate enters the Tricarboxylic Acid Cycle (TCA) in the form of α-ketoglutarate to generate energy. While normal cells mostly consume glutamine to generate energy, invasive breast cancer cell lines, characterized by high levels of the Xc glutamate-cystine antiporter, secrete large amounts of glutamate in the extracellular space. Excess of glutamate in the extracellular compartment activates on the surface of breast cancer cells, likely through a paracrine effect, the metabotropic glutamate receptor GRM3 that, in turn, triggers recycling of the protease MT1-MMP, via a Rab27-dependent pathway, to active invadopodia, thereby allowing matrix degradation and invasion [22]. This is one example, and many others have been provided, of how metabolic rewiring not only sustains tumor growth and survival, but also promotes the acquisition of invasive properties. In this context, proline catabolism has also been found to increase in breast cancer metastasis stimulating metastatic dissemination [23]. Moreover, metabolic plasticity has been shown to create the favorable mileu for the formation of the metastatic niche. This is due to increased pyruvate metabolism in cancer cells that stimulates the production of mature collagen in the stroma supporting homing of breast cancer cells [24]. Recently, a growing body of evidence points to a critical role for fatty acid metabolism in breast cancer development. Indeed, high lipid metabolism provides a reserve of fuel to be exploited under nutrient deprived conditions. Moreover, lipids are the major structural components of the

cellular membrane system, and they also serve as second messengers in the signaling cascade [25]. Breast cancer cells can increase lipid metabolism by multiple means. They can scavenge fatty acids from the environment by increasing their plasma membrane transporters. Moreover, activation of oncogenic signaling, primarily the PI3K/AKT/mTOR pathway, potentiates lipid production by stimulating the activity of key enzymes in the *de novo* lipogenesis pathway [14]. The hormone receptor positive tumors preferentially activate de novo lipogenesis and fatty acid oxidation, while the TNBCs express genes involved in the exogenous lipid uptake and storage [26]. Lipid storage occurs in a dedicate organelle named the lipid droplet (LD).

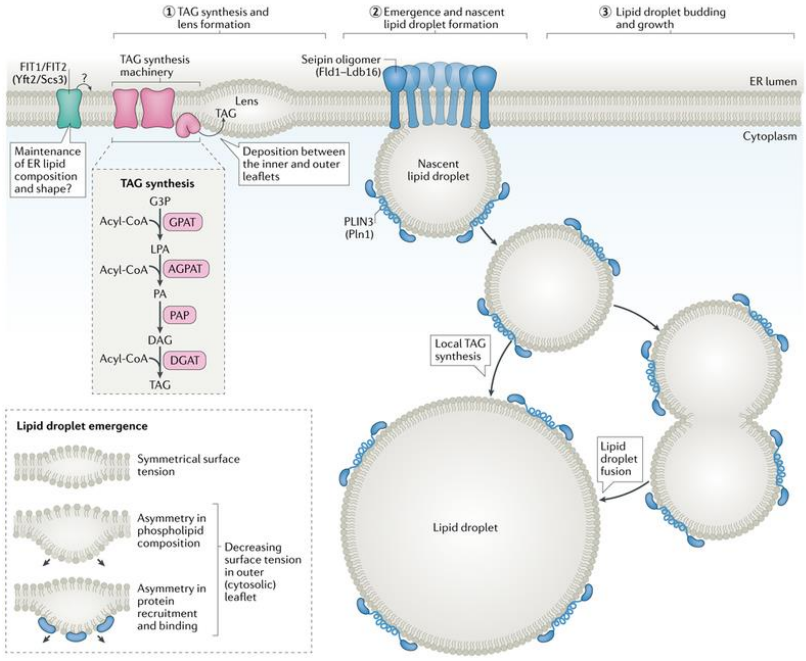

Figure C: Representation of the three main steps in lipid biogenensis. Starting from the the deposition neutral lipids in between the ER, to the lipid droplets budding [27]

LDs are highly dynamic. They grow when lipids are abundant and are consumed through enzymatic hydrolysis (lipolysis) or autophagy (lipophagy) during starvation for energy production [27].

Lipid droplets are generated in the Endoplasmic reticulum (ER) where triacylglycerols (TAGs) are synthesized by sequential addition of fatty acids

to a glycerol backbone. First, enzymes localized on the ER membrane generates neutral lipids after encountering their substrates (for instance fatty acyl-CoA produced by acyl-CoA synthetase (ACSL) enzyme). Neutral lipids start to accumulate at the ER membrane generating a lipid lenses. Above a certain size, and depending on the oil and phospholipid composition, lipid lenses in the ER became unstable and bud. The smallest mature cytosolic LDs have diameters in the range of 250–500 nm. LDs growth occurs by the local synthesis of TAGs on the surface of LDs which occurs by delivery of enzymes necessary for TG synthesis to LDs. Both nascent and mature LDs can acquire enzymes for their growth from the ER [28]. Several components have been found to regulate ER-lipid droplets contacts including DGAT2 which pairs with fatty acid transporters, RAB18 with SNAREs and cortical ER proteins. However how LDs are formed and detach from the ER is still not completely understood. Deletion of these components has different effects according to the cell line, indicating that tethering mechanisms for lipid droplets might be context-specific [27].

Lipid droplets have also been found, not only to sequestrates free fatty acids, but also unfolded or misfolded proteins to alleviate ER stress. Cells require lipid droplets for protection against lipotoxicity in a variety of stressful conditions, including during lipid overload, hypoxia and oxidative stress, high autophagic flux and dysfunctional lipolysis [29]. The same mechanisms that regulate autophagy give rise to lipophagy, induced by the major metabolic kinases mTORC1 and AMPK during lengthy fasting. How fusion between lipoautophagosomes and lysosomes occurs is unknown, however, it includes soluble factors such as N-ethylmaleimide-sensitive factor attachment protein receptors, microtubule-associated protein light chain 3 (LC3), LAMP1, LAMP2B and LAMP2C as well as small GTPases, such RAB7A [30]. Lipophagy has also an important role in adipogenesis and lipid synthesis as binding of phosphatidylethanolamine-conjugated LC3-II to LDs activates both anabolic and catabolic processes [30].

2.3 Membrane trafficking in the regulation of cell metabolism, RAB GTPases and their negative regulators, the RabGAPs

The majority of processes occurring in the cell rely on membrane trafficking events, i.e. on the biogenesis, movement, and fusion of vesicles. Membrane trafficking, by regulating delivery to the plasma membrane, endocytosis, recycling and degradation of a variety of receptors and cargoes controls several events including signal transduction, directional migration, cell division, and differentiation that are frequently subverted in pathological conditions [31]. Recently, membrane trafficking has been implicated in the regulation of cell metabolism thanks to its effect on the stability and subcellular localization of nutrient transporters and metabolic enzymes that impact on the metabolic homeostasis of the cell [32]. Both in unicellular and multicellular organisms the endocytic trafficking regulates a wide range of metabolic phenomenon. For instance, membrane traffic of receptors such as insulin and glucagon receptors modulate hormonal signaling in target tissues. Furthermore, there is a reciprocity on how cell metabolism can regulate membrane trafficking signals. Lacks of nutrient such as glucose can trigger changes in the activity of signaling cascades [32].

Several examples point out the complexity of interdependence of metabolic signals and membrane traffic. Crosstalk between kinase in the AMPK/mTOC1 signaling pathway might be altered by nutrient sensor in various tissues. AMPK controls the activity of glucose transporters such as GLUT1 and GLUT4 enhancing glucose uptake to sustain metabolic requirements. While amino acids or lipid sufficiency can result in the recruitment and activation of mTORC1 [33] .

Membrane trafficking is regulated in space and time by the activity of the RAB GTPases (RABs). RABs are small GTP binding proteins that mark distinct vesicular compartments; just to mention few examples: RAB5 localizes to early endosomes, RAB7 on late endosomes, multivesicular bodies and lysosomes, RAB1 and RAB2 are found in the cis-Golgi [25]. In humans, RABs form a wide family with more than sixty-three members. They cycle between a GTP-bound active state to a GDP-bound inactive

form. This cycle is tightly regulated by GDP/GTP exchange factors (GEFs) and GTPase activating proteins (RabGAPs) [34]. Membrane trafficking can be divided into four steps: I) Budding of the nascent vesicle, characterized by the sequestration of the cargo to a specific region of the donor membrane; II) Transport, in which the vesicle containing the cargo is delivered to the target compartment; III) Tethering, when the vesicle arrives in proximity of the acceptor membrane; IV) Fusion, when the vesicle fuse with the acceptor compartment releasing its content [35]

Several studies have shown that RABs control vesicles budding, interaction with the cytoskeleton, and tethering/docking to their target compartment. RABs might both directly or indirectly influence the assembly of the vesicles coat components or help the incorporation of cargo molecules. A crucial aspect of their function is the coordination between the vesicle tethering/docking and the SNARE-dependent membrane fusion [36].

Different RABs act in a coordinated fashion to synchronize membrane trafficking events. Four main types of crosstalk among RABs have been identified:

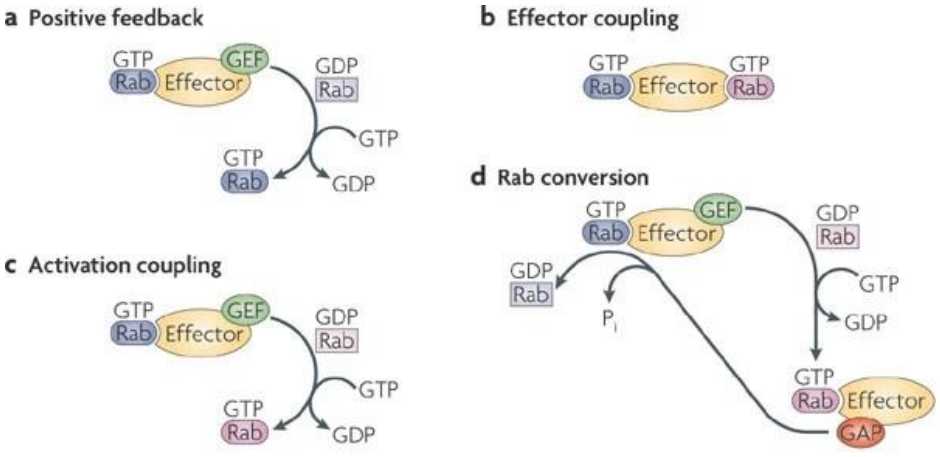

Figure D: Different activation of Rab functions. Each of the four schemes represent a possible Rab GTPase/ GEF coordination on the GTP/GDP switch on effector molecules [34]

1) The positive-feedback loop. This is the condition in which the RAB binds to an effector that interacts with a GEF that, in turn, activates the RAB itself.

2) The effector coupling. This occurs when the effector binds to two distinct RABs enabling tethering of two membranes.

3) The activation coupling. This happens when the RAB effector presents a GEF for a second RAB GTPase.

4) The Rab conversion. In this case the upstream RAB binds to its effector that brings a GEF for a downstream RAB, thus activating this second RAB. The downstream RAB binds to a GAP for the upstream RAB, thus turning it off [34].

As mentioned above, inhibition of RAB activity is achieved by the RabGAPs that stimulate hydrolysis of GTP on the RAB target. In humans, the RabGAPs form a large family of fourty-five members all sharing an enzymatic GAP domain named the TBC domain because it was initially identified in the Tre2, Bub2, Cdc16 proteins [37]. The mechanism of catalysis of the TBC domain relies on the presence of two catalytic fingers that terminate respectively with an arginine and a glutamine residue [38].

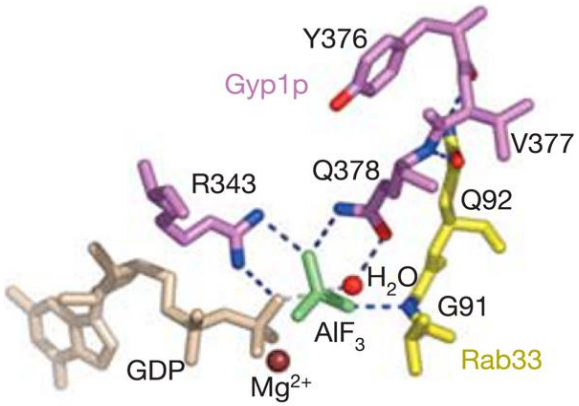

Figure E: Mechanism of action of the TBC-GAP domain. It has been revealed by David Lambright who solved the crystal structure of the complex between Rab33 and the GAP Gyp1. Here is a detail of this complex crystallized in presence of aluminium fluoride, which approximates the transition-state intermediate for GTP hydrolysis. This crystal structure reveals that the GAP protein provides two fingers (here in pink), which terminate respectively with an arginine and a glutamine, that accelerate the hydrolysis of GTP on the RAB. In yellow are the residues belonging to the Rab, in particular this glutamine seems to have a key role in binding to the GAP [38]

However, fifteen RabGAPs carry an enzymatically inactive GAP domain, which lacks one or both the two catalytic fingers and, therefore, these RabGAPs are classified as GAP-defective or GAP-dead [39].

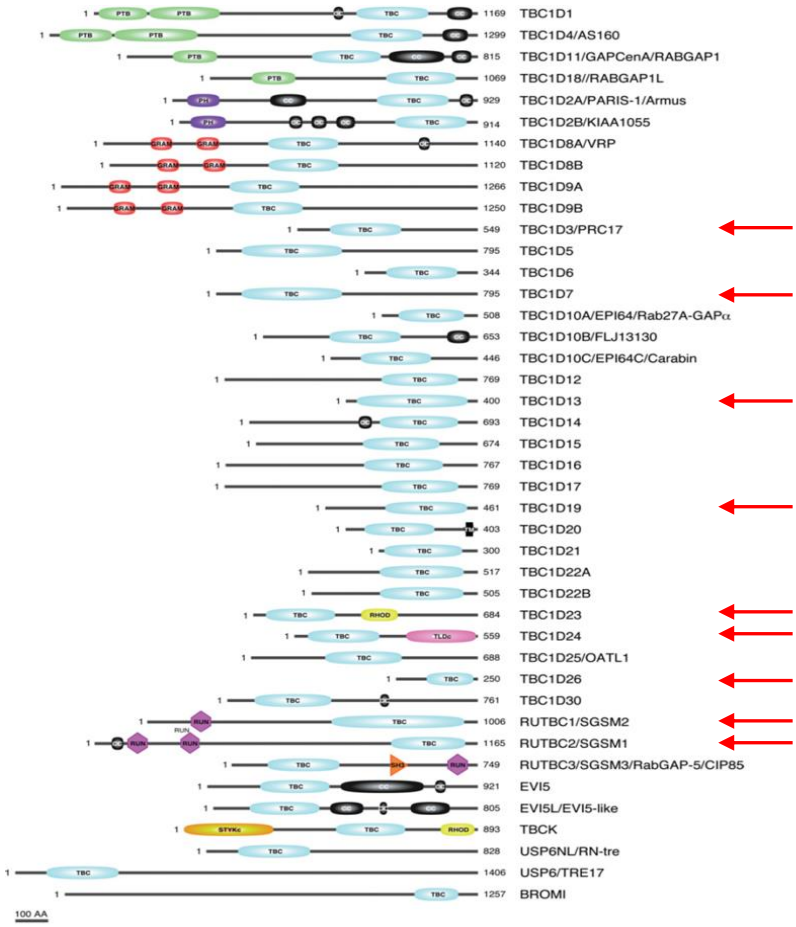

Figure F: The human RabGAP family. The TBC-GAP domain is in blue. The red arrows point to GAP-defective or GAP-dead protein [37]

The RabGAPs are known to be promiscuous enzymes since they can inactivate multiple RAB targets. Moreover, the opposite is also true: a single RAB can be regulated by more than one RabGAP. Because these enzymatic interactions regulate fundamental cellular functions, they generate a complex network protein-protein interactions of effector and regulators showing different spatial distribution [39]. The figure below illustrates a map of experimentally validated interactions between members of the RAB and RabGAP families. For instance, USP6NL has been found to act both on Rab5 and Rab43 [40]. Similarly, some RABs, like RAB35, can be regulated by more than one RabGAP. Interestingly, some RabGAPs can bind to the RAB without stimulating GTP hydrolysis as for RUTBC2 which

binds to Rab9 but exerts its GAP activity on Rab36, thus linking the trafficking events mediated by these two GTPases [41].

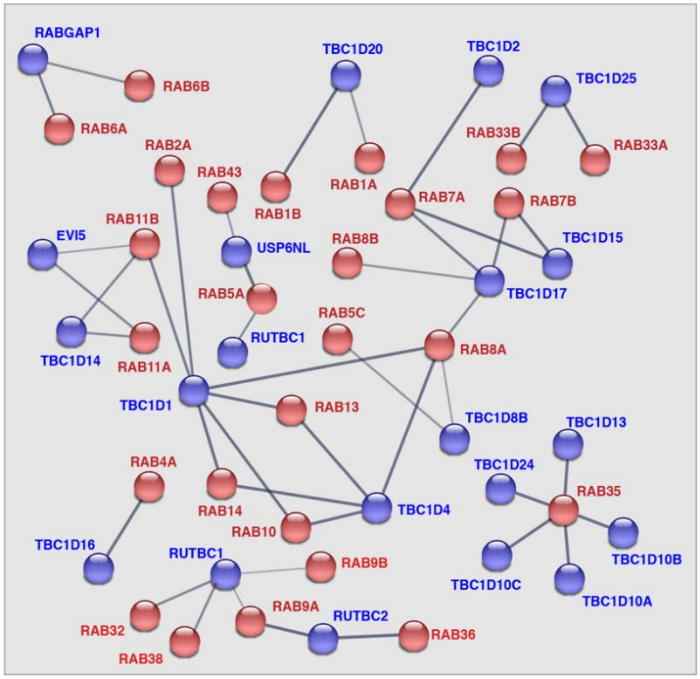

Figure G: RabGAP can have multiple RAB targets. Similarly, RABs can be regulated by more than one RABGAP. Manually curated STRING analysis https://string-db.org RED: Rabs BLUE: RabGAPs

It is worth noticing that the interaction between RAB GTPases and RabGAPs are integrated in a wide signaling network and crosstalk with other GTPases.

By inhibiting the activity of RAB GTPases, RabGAP proteins control vesicle budding, motility and fusion participating to membrane trafficking regulation of biological processes including cell metabolism. In this context, two RABGAPs, TBC1D4 and TBC1D1 have been shown to restrain the delivery to the plasma membrane of glucose transporters thereby inhibiting glucose uptake and glycolysis [42]. Most of the RabGAPs found to be involved in the regulation of cell metabolism participate to the scavenging pathways macropinocytosis (TBC1D3 and USP6NL) [43] [44] or autophagy (TBC1D14, TBC1D5, TBC1D7, TBC1D20), [45]–[47] which can replenish the metabolic building blocks thus helping cells to survive under nutrient deprived-conditions. While the function of membrane trafficking proteins in

the physiological regulation of cell metabolism is a long-standing notion, little is known about the involvement of RabGAP proteins in the pathological alteration of cancer cell metabolism. Recently, our laboratory has contributed to the study of the involvement of RabGAP proteins in cancer cell metabolic reprogramming by finding that high level of USP6NL correlates with elevated glycolysis and poor prognosis in breast cancer [48]. High levels of USP6NL inhibits Rab5, limiting the endocytosis of the EGFR which, in turn, causes prolonged PI3K recruitment and AKT phosphorylation. This sustained AKT activation stabilizes the glucose transporter GLUT1 to the plasma membrane elevating glycolysis [48]. This endocytosis-based mechanism of glycolysis elevation further indicates the crosstalk between membrane trafficking and cancer cell metabolic reprogramming.

2.4 RAB GTPases in the regulation of Golgi transport

The Golgi complex is characterized by differently shaped membrane sub compartments called cisternae.

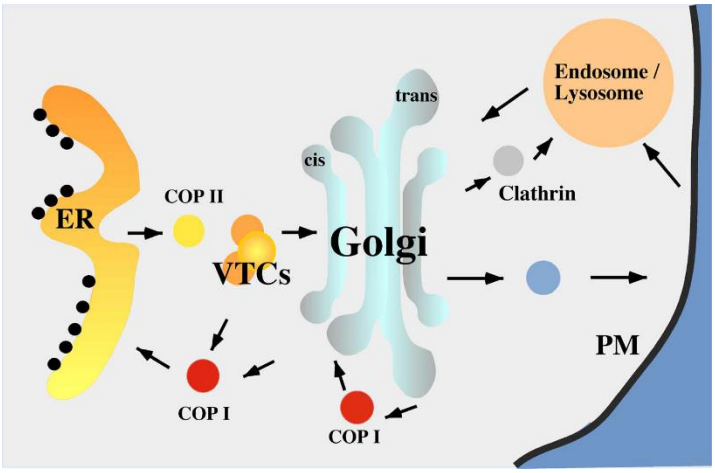

Three distinct arrangements can be identified: the cis Golgi, the medial Golgi and the trans Golgi (TGN) [49].

Figure H: Schematic representation of vesicles transport from Endoplasmic reticulum (ER) to vesicula-tubular clusters (VTCs), to Golgi/Endosome/Lysosome. Involvement of COP I, COPII and clathrin coated vesicles is shown [50] .

The Golgi apparatus receives newly synthetized molecules from the Endoplasmic Reticulum (ER). Here, they are modified, mostly by glycosylation, as they transit from the cis to the trans Golgi. Once they leave the Golgi, they can enter the secretory pathway and move toward the

plasma membrane (PM). This transition is known as the anterograde pathway. In the retrograde transport, the vesicles move from the Golgi back to the ER [49]. Despite continuous trafficking, each compartment is characterized by specific resident molecules. Vesicles moving through these compartments are coated by specific molecules: the COP I and COP II complexes [51].

Remarkably, about one third of known human RABs have been found associated with membranes of the ER and Golgi where they regulate structure and homeostasis of these membrane compartments [36], [52], [53]. Different RABs are localized to specific membrane subdomains. RAB1 is one of the main players of the cis Golgi. The active GTP-bound form of the protein specifically binds to GM130 [54], while its functional ablation causes Golgi disruption [55]. RAB1 exists in two isoforms (RAB1A and RAB1B) encoded by distinct genes showing high percentage of similarity. Among the known TBC proteins, TBC1D20 was found to possess a transmembrane anchor that target it to the ER and cause Golgi disruption upon overexpression.

Being localized to the ER thanks to the activity of the reticulons, and functioning on Golgi stabilization, TBC1D20 was hypothesized and later demonstrated to act as a GAP on both RAB1 and RAB2 [55].

Initial studies on RAB1B activity showed that this protein can regulates early steps of the ER and the cis-Golgi transport. Moreover, RAB1B was found to be involved in another stage of vesicular trafficking, from cis to medial-Golgi compartment [56]. The RAB1 mediated regulation ER-to-Golgi transport resides on the ability of the protein to recruit p115 onto budding COPII vesicles where p115 can directly interact with the SNAREs proteins. In this manner COPII vesicles are directed for delivery to the Golgi membranes [57].

Later studies demonstrated a synergy of RABs activity; showing that more than 60% of vesicular carriers contains both RAB1B and RAB6A [58].

The role of RAB1B in breast cancer have been supported by the findings that this Rab GTPase can regulate the degradation of the TGF-β receptor 1

(TβR1) [59]. Depletion of RAB1B inhibits the activity of TβR1 resulting in an increased TGF-β signalling. Since TGF-β is known to promotes invasion and metastasis in cancer, the role of RAB1B in controlling downstream TβR1-SMAD3 cascade point out the importance of this molecule in the regulation of the early stages of EMT/invasion [59].

Another striking aspect is the correlation between RAB1B and a phosphatidylinositols (PIs) family member: PITPNC1 [60] PITPNC1 was found to be overexpressed in a variety of human cancers, correlating with worst prognosis in breast tumor. PITPNC1 forms a complex with RAB1B at the TGN/Golgi level, binding to the Golgi-resident lipid PI4P, thus coordinating Golgi morphology. Indeed, enhanced P14P levels increase the amount of P14P binding molecule, GOLPH3, responsible of the regulation of Golgi morphology. Interestingly, Golgi structure and maintenance is thought to be a key feature of highly metastatic cells [60].

On the other hand, the RAB1A isoform can respond to amino acid signaling by regulating mTORC1 kinase activity. RAB1A does not directly interact with mTORC1 but uses the Golgi as an anchor to regulate Rheb, but not Rag, mediated activation of the kinase cascade [61]. This suggests that RAB1A and Rag are active on two independent routes of mTORC1 activation. For this reason, as expected, RAB1A knockdown blocks Rheb-mTORC1 interaction on the Golgi, not affecting the activity on the lysosome mediated by Rag [61]As a result, RAB1A has been found to be overexpressed in several human malignancies such as tumors or cardiomyopathy [61].

Many RABs have also been found associated to the late Golgi/TGN. Among them, RAB6 is the most abundant and well-studied. The RAB6 family include four proteins: Rab6A, Rab6A', generated by alternative splicing, Rab6B and Rab6C [62]. Numerous studies established the importance of RAB6A/A' in both the retrograde transport between endosomes and ER and in the anterograde transport between Golgi and PM [49]. How RAB6 is regulated is still debated. GAPCenA, also known as RABGAP1 or TBC1D11, was initially proposed to be the RAB6A RabGAP [63] but later studies have shown that controls the activity of RAB4 [40]. Instead, GTP

loading on RAB6A by Guanine nucleotide exchange factors has been found to rely on the activity of the complex formed by Ric1 and Rgp1. Depletion of these two proteins causes Rab6A inactivation and interferes with the retrograde transport. In addition, both Ric1 and Rgp1 can associate with each other and independently bind to Rab6A-GDP [64].

RAB6A has also been found to control the mechanisms that drives most of the post-Golgi secreted molecules to exocytic spots closely related to focal adhesions (FA) [65]. The specific targeting to FAs of the newly secreted cargoes does not depend on the function of the cargo itself, but rather on the presence of factors necessary for docking/fusion of transport carriers. Among them RAB6 is likely one of the major regulators of post-Golgi transport by regulating the core machinery that drives secretion on exocytic hotspots close to FAs. This existing link between Golgi membranes and FAs results in the regulation of cellular polarization and migration [65]. A related activity is the ability of RAB6A to regulates the fission of positive post-Golgi secretory vesicles to preferential sites [66] In fact, RAB6A participates to KIF20A recruitment to Golgi/TGN membranes in presence of myosin II, allowing the clustering of molecules to microtubules (MTs) [66].

2.5 The RabGAP protein TBC1D22B

We investigated the RabGAP family looking for members that participate to the elevation of glycolysis in breast cancer cell. Among them, we selected those that showed increased expression in breast tumors correlating with worse prognosis. One of the best targets of these two combined approaches was TBC1D22B (detailed in the Result section paragraphs 5.1 and 5.2), a still uncharacterized RabGAP that localizes to the Golgi complex. In human cells, two isoforms of TBC1D22 exists (TBC1D22A and TBC1D22B) which are encoded by distinct, highly homologues, genes. Both TBC1D22A and B have been shown to participate to the maintenance of the ER-Golgi intermediate compartment (ERGIC) [55] . Their overexpression causes both ERGIC disruption, with TBC1D22B having a stronger impact, and Golgi fragmentation, even if this latter effect seems to be cell context-dependent

[55]. Their role in maintenance of the ERGIC and Golgi structures is dependent on their GAP activity indicating that, by inhibiting one or more RAB GTPases they control the homeostasis of these compartments [55]. Currently, the RAB target(s) of the GAP activity of TBC1D22A and B are unknown. These RabGAPs have been proposed to act on the GTPase RAB33, even if this has not been experimentally proven. In addition, both TBC1D22A and B have been shown to binds to the multifunctional Golgi adaptor acyl coenzyme A (acyl-CoA) binding domain protein 3 (ACBD3/GCP60) [67] which is involved in Golgi structure maintenance [68]. Interestingly, ACBD3 is highly expressed in the more aggressive breast cancers and its upregulation promotes self-renewal and tumorigenesis of breast cancer cells via the activation of Wnt/beta-catenin signalling [69]. More recently, ACBD3 has been shown to control ER to Golgi transport of STING, a specialized receptor responsible for eliciting the type-I interferon signalling at the Golgi. Interestingly, this study demonstrates the involvement of ACBD3 in the concentration of non-canonical cargoes at specific ER exit sites [70], a function that might likely involve the TBC1D22 proteins.

Despite TBC1D22A and TBC1D22B share 62% of identity at the amino acid level, important differences in their behavior and function seem to exist. TBC1D22A, but not TBC1D22B, has been shown to regulate surface delivery from the Golgi apparatus of the a2B-Adrenergic Receptor, a prototypic G Protein Coupled Receptor, in a GAP dependent manner [71], suggesting that TBC1D22A could be involved in selective trafficking of cargoes and receptors from the Golgi to the cell surface. Moreover, as detailed in paragraph 5.2, while TBC1D22B is overexpressed in breast cancer correlating with worse prognosis, no alterations have been identified on TBC1D22A in breast cancer patients.

Recently, a role for TBC1D22 in cell metabolism has been revealed in the *Drosophila* model system which carries only one orthologue, *dTBC1D22*.

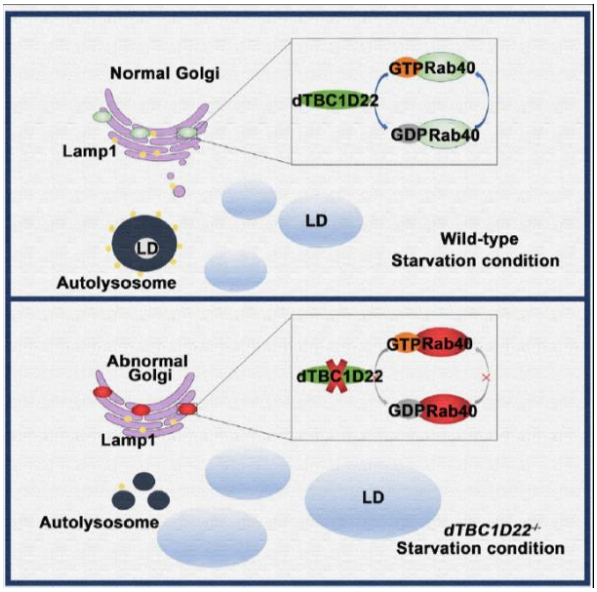

Knocking down *dTBC1D22* increases the production of Lipid Droplets (LD) and this effect is mimicked by mutation of the GTPase Rab40 [72]. Overexpression of this GTPase or its mutants, locked either in the GTP- or GDP-bound state also increase LDs formation and lipid mobilization [72].

Figure I: Graphical representation of dTBC1D22 functions as Rab40 GAP in the regulation of lipid homeostasis. Rab40 is shown to localize to the Golgi together with dTBC1D22B regulating Lamp1 distribution upon starvation. Loss of Rab40 leads to lipophagy defects [72].

While the study on the Drosphila TBC1D22 ortologue points to RAB40 as a target for this GAP, in humans the regulation might be more complex since gene duplication has produced two TBC1D22 molecules and four RAB40 GTPases.

2.6 The Proximity Biotinylation technique as a tool to identify transient enzyme-based protein networks

Enzymatic reactions, such as those involving RAB GTPases and RabGAPs occur within seconds in the cell and are based on the transient interaction between the two proteins. Once the GTP is hydrolyzed to GDP on the RAB, the interaction is released [38] . Standard biochemical techniques such as co-immunoprecipitation are not designed to identify protein-protein interactions based on enzymatic reactions. To overcome this limitation, different techniques have been developed, including proximity biotinylation, which is one of the most versatile in revealing transient interactions and networks of neighboring proteins [73].

In the proximity biotinylation assay, biotin is covalently attached to the proteome of interest which can be subsequently recovered by streptavidin pull down and identified by mass spectrometry. Biotin attachment is provided by the engineered version of the soybean peroxidase APEX. APEX is a 27kDa monomeric domain, free of disulphides bonds, that contains a noncovalently bound heme cofactor in its active site [74].

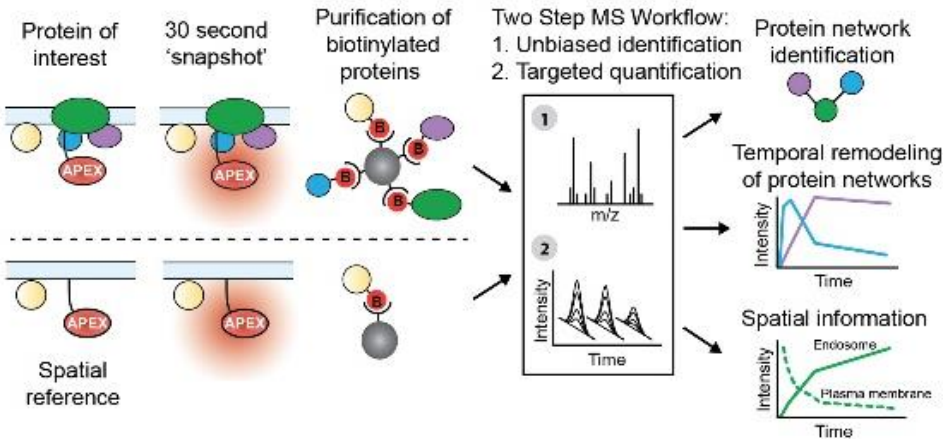

Figure L: Workflow to identify the interacting network of the protein of interest employing APEX2. 30 seconds biotinylation labelling allows for the purification and subsequent identification of the local proteome. A two-steps mass spectrometry analysis compares temporal and spatial remodeling of protein network [75]

APEX2 uses hydrogen peroxide (H_2O_2) as an oxidant to catalyse the one-electron oxidation of a diverse set of small-molecule substrates. The substrate that is relevant for proteomics is biotin-phenol. In presence of hydrogen peroxide, APEX2 converts it in the highly unstable and short-lived (< 1ms) biotin-phenol radical that conjugates to the proximal molecules. The attachment of biotin to the neighbouring molecules occurs within a radius of around 20 nm, a distance compatible with protein-protein interactions [73]. Biotinylated proteins are then pull down by streptavidin and identified by shotgun mass spectrometry. The initial version of APEX was a triple mutant of the wild-type soybean ascorbate peroxidase. Stability and specificity were improved by adding one mutation, thus generating the updated version: APEX2 [74]. APEX2 presents improved kinetics, thermal stability, heme binding and resistance to high H_2O_2 concentrations [75]. It can be fused to

the protein of interest and the resulting chimera expressed in cells biotinylates the interacting/neighboring proteins. The specificity of the proteome isolated by this technique strongly depends on the proper subcellular localization of the chimera. APEX2 has also been successfully employed to identify the networks of proteins that characterize distinct subcellular compartments thanks to its specific targeting to the compartment of interest by peptide tagging [75]–[79].

One of the advantages of using APEX2, compared to other tagging systems, is that protein biotinylation is achieved upon treatment with H_2O_2 for one minute or less. This allows to follow the activity of the tagged protein with high spatial and temporal resolution [75]. This technology, therefore, represents a powerful tool to answer three fundamental questions concerning biological process: what, when and where.

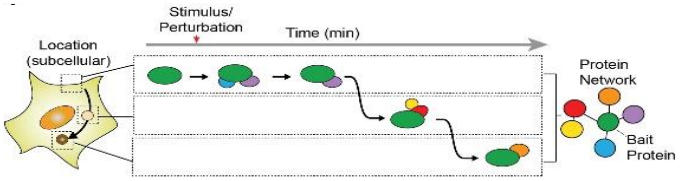

Figure M: Subcellular localization and interacting network theory due to stimulus/perturbation in APEX2 overexpressing cells [75]

Two are the major applications of this technique:

1) It can be exploited to investigate the spatial formation of protein complexes at the subcellular level by immunofluorescence, either with standard techniques or by electron microscopy;

2) It allows the enrichment and identification of by mass spectrometry protein networks at steady state, or under differently treated conditions [73].

Beside the identification of protein networks, this method has been recently modified and developed to biotinylate and sequence the RNA (APEX-seq) to obtain a spatial resolution map of the human transcriptome [80].

Based on the ability to capture transient interactions, we used proximity biotinylation to identify the TBC1D22B interactome as detailed in the Result

section. This technique has already been successfully employed to identify RAB-dependent interactomes. Four RAB GTPases have been tagged with APEX2, RAB4, RAB5A, RAB7A and RAB21 revealing the effectors and regulators that characterize their interactomes [81].

3 Materials and Methods

3.1. Cell cultures and siRNA-mediated silencing

BT549 and MDA-MB-468 were grown in RPMI (Sigma) supplemented with 10% FBS (Euroclone) and 1% glutamine.

In the silencing experiments, cells were plated in six-well plates or twenty-four-well plates as indicated in the table below.

Cell line	Twenty-four well plates	Six-well plates
MDA-MB-468	30000/25000	220000
BT549	25000	200000

The first day cells were counted and plated in presence of 50 pmol of siRNA oligos (reverse silencing), and a second round of transfection was repeated with other 50 pmol of siRNA oligos the day after on the adherent cells. 1.5 µl of control oligo and 2 µl of targeting oligo were used for silencing experiments in six-well plates, while 0.6 µl and 1 µl of control and targeting siRNA oligos respectively were used for twenty-four-well plates experiments, corresponding to 10 pmol. Functional ablation of TBC1D22B and RABGTPases were performed with a pool of four oligos purchased from Dharmacon. Cells were harvested 72 hours after the second silencing transfection.

3.2 Plasmids and generation of stable cell line

The cDNA of TBC1D22B was inserted in the lentiviral pLV backbone fusing its N-terminus in frame with the cDNA of APEX2. To generate the GAP-defective TBC1D22B mutant, we mutagenized the two catalytic residues,

arginine 274 and glutamine 309 (TBC122BRQ). A myc tag was added at the N-terminus of APEX2, while an HA tag was fused to the N-terminus of the TBC construct, all these sequences were in frame. We inserted an XhoI site right after the ATG of the myc tag and another XhoI site was added right before the HA tag. This allowed us to remove the myc-APEX2 sequence by digesting the construct with XhoI thus obtaining the HA-tagged version of TBC1D22B in the pLV vector. The GAP-defective mutant was designed and processed in the same way.

Puromycin-resistant stable cell population expressing these constructs were obtained by infecting the BT549 cell line with viruses produced in HEK293T cells. Constructs employed in the RUSH experiments were: Li-Str_SBP-EGFP-GPI (Addgene 65296) and Str-KDEL_SBP-EGFP-GPI (Addege 65294) gifted by Franck Perez Laboratory.

The GST version of the proteins employed in the GAP assay were purchased by Addgene: GST-RAB6A (49567), or VectorBuilder: GST-TBC1D22B, GST-TBC1D22B, GST-RAB1B, GST-RAB13 and GST-RAB35.

The GST-tagged version of the protein was inserted into the pET vector, under the control of the T7 promoter which drives high-level transcription. Both Lac operator (LacO) and repressor (LacI) were inserted in order to regulate downstream protein transcription. In presence of IPTG, LacI can no longer binds LacO thus allowing adjacent gene transcription. Ampicillin resistance was inserted to select expressing-vectors bacteria.

3.3 Measurements of intracellular Lactate concentration

MDA-MB-468 cells were plated in 24 well-plates and transiently transfected with the pool of four oligoes for TBC1D22B or with the non-targeting oligo as control, as already described in paragraph 3.1. Intracellular lactate production was evaluated using the Lactate-Glo Assay (Promega).

The assay is based on a bioluminescent reaction which couples lactate oxidation and NADH production with the generation of bioluminescent signals. Lactate dehydrogenase provided by the kit uses lactate and NAD+

to produce pyruvate and NADH. The reductase (also provided) utilizes the NADH to convert pro-luciferin in luciferin resulting in the release of light signal. The luminescent signal is proportional to the amount of NADH produced, which in turn corresponds to the amount of lactate in the sample and continuously increase until lactate is completely consumed. From this point on the signal reaches a plateau and remains stable.

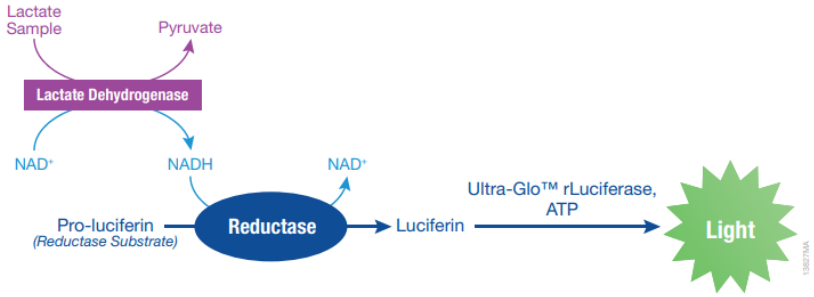

Lactate was extracted from silenced cells. Cell media was removed and cells were washed with PBS. Inactivation solution made with fresh PBS supplemented with 0,6N of HCl was add to the cells. Neutralization was done adding 1M TRIS base. 50µl of sample were transferred into a 96-well plate. A negative control corresponding to buffer only was included to determine the assay background. The detection reagent (containing Lucierin Detection solution, Reductase and Reductase Substrate, Lactate Dehydrogenase and NAD) was added, and after 60 minutes, plate was read using the Tecan Spark10M. A calibration curve was generated in each experiment and used to derive the corresponding concentration of intracellular Lactate. Following lactate extraction cells nuclei were fixed in PAF 4% for 10 minutes and stained with DAPI. To assess the number of cells per well. Plates were then acquired using Cytation3 Imaging Reader and images were analyzed using Imagej program. To obtain the amount of intracellular L-lactate in pmol per cell, the amount of lactate obtained was normalized over the number of cells.

3.4 Seahorse analysis

Two distinct parameters: ECAR (Extracelluar Acidification Rate) and OCR (Oxygen Consumption Rate) have been measured employing the XF96

Extracellualr Flux Analyzer purchased by Agilent. MDA-MB468 cell line have been silenced using non-targetting siRNA oligo as control (siCTR) or TBC1D22B siRNA in 6 multiwell plates. Three days after silencing, cells were harvested and plated in XF96 plates (6 well per condition, 20000 cells/well) and incubated for 24 hours. Cells were incubated at 37°C without CO_2 for 60 minutes before the experiment. Glycolysis was evaluated by treating cells with Glucose 10mM, Oligomycin 1 µM and 2DG 50mM; while for Mitochondrial respiration cells were treated with Oligomycin 1 µM, FCCP 1 µM and Rotenone/Antimycin A 0.5 mM. All treatments were done in presence of DMEM medium supplemented with 2mM Piruvate, 1mM Glutamine at pH 7.4. Plates were washed in PBS and fixed with PAF 4%. After DAPI staining, cells were counted using Cytation 3. Each value was normalized over the cell number.

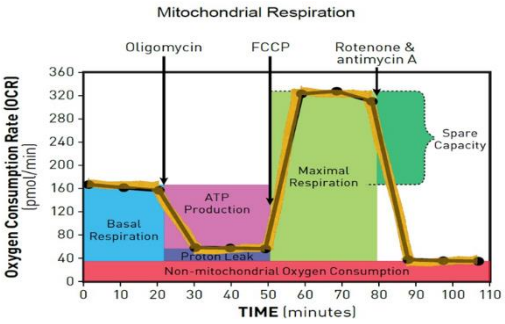

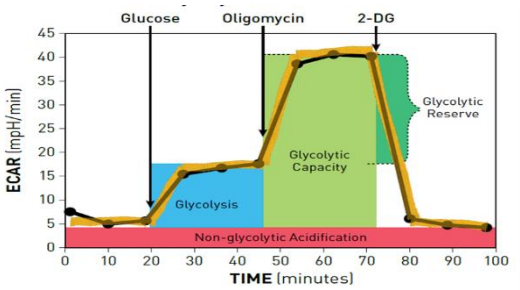

3.5 Proliferation Assay

Cells were plated in six-well plates and silenced as previously described in 3.1. paragraph. Six hours after the second round of transfection, cells were detached and 15000 cells-well were plated in 48 well-plates. After 18 hours the time zero is stopped by fixing cells in PAF 4%, while medium is changed in the other conditions. Following time points (24h, 48h and 72h) were stopped at the same time of medium changing. Cells were stained with DAPI and plates were acquired using Cytation3 Imaging Reader. To assess the cell number, images were analyzed using Imagej program. Results were normalized over the corresponding time zero.

3.6 Glucose uptake

Cells were plated in 24 well-plate and silenced as described in 3.1 paragraph. Glucose uptake was evaluated on silenced cells employing the "Glucose Uptake-Glo™ kit (J1341, Promega), following manufactures instructions. Cells were starved in RMPI w/o FBS and glucose for 4h before performing the experiment.

Reagent Preparation was performed as follow:

Component	**Per Reaction**	**Per 10ml**
Luciferase Reagent	100µl	10ml
NADP+	1µl	100µl
G6PDH	2.5µl	250µl
Reductase	0.5µl	50µl
Reductase Substrate	0.0625µl	6.25µl

Medium was removed and cells were washed in 100µl PBS. 250µl of the prepared 1mM 2DG per well was added, plates were shake briefly, and incubated 10 minutes at room temperature. 125µl of Stop Buffer were added followed by 125µl of Neutralization Buffer. 50µl of sample were transferred to 96-well plate and 50µl of 2DG6P Detection Reagent were added. Plates were shake and incubated at room temperature for 1h. Luminesce were recorded using "Glucose Uptake-Glo™" program on GloMax® instrument. A calibration curve was generated in each experiment and used to derive the corresponding glucose concentration. Resulted rate of glucose uptake was calculated applying the formula:

([2DG6P] × (volume of sample)) ÷ ((number of cells) × (time of uptake))

Number of cells was evaluated following DAPI staining as previously described in this paragraph.

3.7 Correlation between gene expression and clinical-pathological parameters in the Metabric dataset

Clinical data and data for Copy Number Alteration (CNA, 1904 samples) or RNA expression (1909 patients) were downloaded from the cBioPortal for Cancer Genomics [82] and from The European Genome-phenome Archive https://ega-archive.org/ (EGAD00010000210, discovery set, 997 samples; EGAD00010000211, validation set, 995 samples). For each Gene UP- or DOWN-regulation was calculated with respect to its average expression. Data were then imported in JMP (version 14.2, SAS Data analysis software) and Hazard Ratios for Death for Breast Cancer calculated with the Cox proportional hazard method. Multivariable hazard ratios were estimated with a Cox proportional hazards model, adjusted for Grade, Tumor Size, Lymph node status, HER2 amplification status and Hormonal Status (ER and PgR combined).

3.8 Proximity Biotinylation and Mass Spectrometry

Cells were plated in quadruplicate as described in the table

Cell line	10cm dish
BT549	3000000

24 hours later, 2 dishes per condition were treated with biotin-phenol (Iris Biotech GMBH, LS-3500.0250) 2mM (BP, diluted in RPMI 10% FBS, 12 ml per dish) for 30 min at 37 °C. H_2O_2 0,2 mM in PBS was added to the medium for 1 minute at RT. Cells were placed on ice and immediately washed three times with the quencher solution (10 mM sodium ascorbate, 5 mM Trolox and 10 mM sodium azide solution in PBS). 1ml of fresh quencher solution per dish was used to scraped cells from the bottom of the well. Cells were pelleted by 10 minutes of centrifugation at 3000xg, 4°C. Pelleted cells were

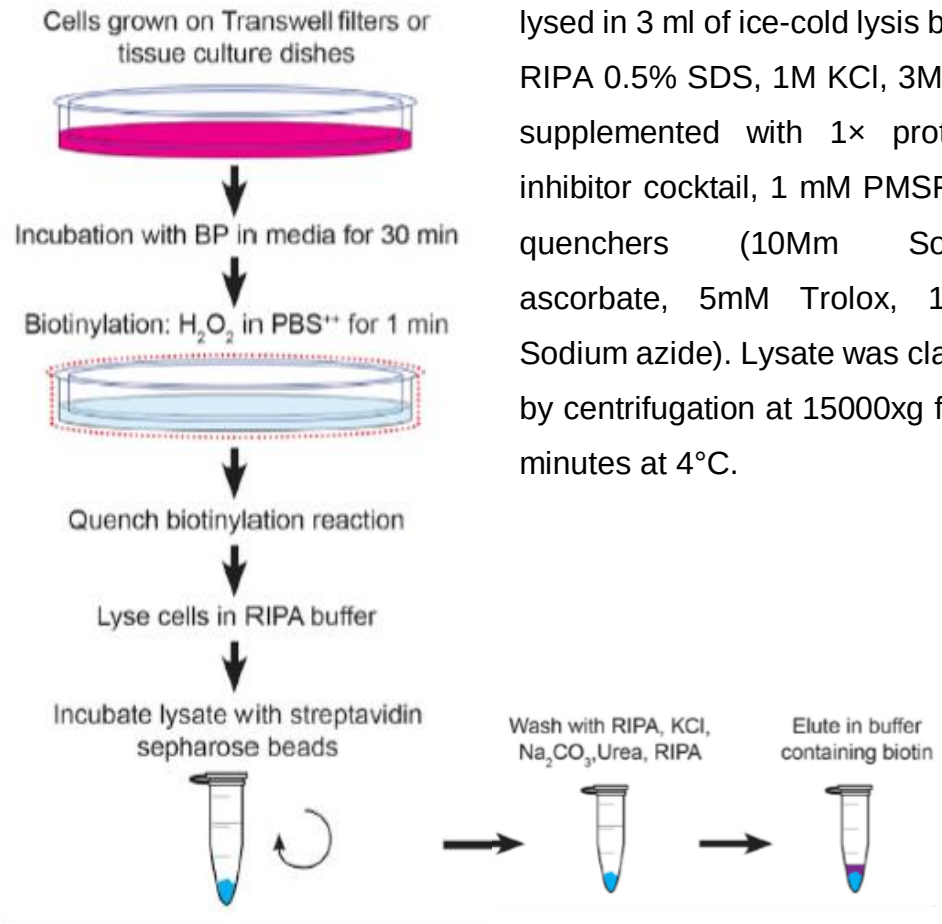

Figure N: Overall Workflow for APEX2-Mediated Proximity Biotinylation [76]

lysed in 3 ml of ice-cold lysis buffer: RIPA 0.5% SDS, 1M KCl, 3M urea supplemented with 1× protease inhibitor cocktail, 1 mM PMSF and quenchers (10Mm Sodium ascorbate, 5mM Trolox, 10mM Sodium azide). Lysate was clarified by centrifugation at 15000xg for 30 minutes at 4°C.

Proteins were quantified with the Bradford method and the same amount of protein per each sample in triplicate (1,43 mg x3 corresponding to a total amount of 4mg of protein lysate) was incubated with 90-µl aliquots of streptavidin magnetic beads (88816, Pierce) slurry 50% for 1 hour at RT.
Beads were then washed using 1ml of each solution as follows:

- Two washes with RIPA 0.5%SDS;
- One wash with 1M KCl;
- Four washes with TBS;
- One wash with 50 mM NH_4HCO_3 3M urea.

After each washing step, beads were recovered using a magnetic stand and supernatant was removed.
One sample was boiled in 60ul of loading buffer and run on NuPAGE 4-12% Bis-Tris Plus to verify biotinylation and recovery. The other two replicates

were dried and frozen at -20°. The experiment was repeated twice obtaining a total of four replicates.

NuPAGE gels were revealed by Colloidal Blue staining (LC6025, Invitrogen). Shaked in Fixing solution 10 minutes at RT. 10 minutes shaking with Staining Solution without Stainer B is followed by the adding of Stainer B. Gel is stained O\N shaking at RT.

Fixing solution	**One Gel**	**Staining Solution**	**One Gel**
dWATER	20ml	dWATER	27,5ml
Acetic Acid	5ml	Methanol	10ml
Methanol	25ml	Stainer A	10ml
		Stainer B	2,5ml

Sample preparation for mass spectrometry was done as follows:

- Reducing step: TCEP 5 mM final (from stock 100 mM 20X add 15 ul) was incubated with orbital shaking, 1 hour 37°C.
- Alkylating step: 2-iodoacetamide 10 mM final (stock 100 mM in H_2O 10X add 33.33 µl) was incubated in the dark with orbital shaking, 20 min RT.
- DTT 20 mM final was added (6.8 µl from stock 1 M in H_2O).
- Buffer was exchanged to 300 µl of 50 mM NH_4HCO_3 3M urea.
- Incubated with trypsin over nigh (no more than 16 hours) at 37°C. Resuspend Trypsin (Promega cat. V5280) 1 µg/ µl in 50 mM acetic acid
- 2.25 µl of trypsin was added to each sample (ratio 1 µg of tripsin in 20 µl beads, ratio v/v 1:200).
- Supernatant was collected
- Beads were washed twice with 60 µl of 50 mM NH_4HCO_3, 2M Urea (pooled the supernatants with the samples). Final volume for each sample was 422.25 µl
- Acidification was performed by adding 1% formic acid (4.22 µl of 100% formic acid).

- Samples we stored at -20°C.

Tryptic peptides were resuspended with 5 µl of 1% TFA, to be then analysed by LC-MS/MS using an EASY-nLC 1200 (Thermo Fisher Scientific) coupled to a Q-Exactive HF instrument (Thermo Fisher Scientific) through a nano-electrospray ion source (EASY-SPRAY, Thermo Fisher Scientific). In all cases, the nano-LC system was operated in one column set-up with an EasySpray PEPMAP RSLC C18 column (Thermo Fisher Scientific) kept at 45°C constant. Solvent A was 0.1% formic acid (FA) and solvent B was 0.1% FA in 80% ACN. Samples were injected in aqueous 1% (TFA) at a constant pressure of 980 Bar. Peptides were separated with a gradient of 3–35% solvent B over 49 min followed by a gradient of 30–60% for 5 min and 60–95% over 5 min at a flow rate of 300 nL/min. The Q-Exactive was operated in the data-dependent acquisition (DDA) to automatically switch between full scan MS and MSMS acquisition. MS spectra (from m/z 375-1650) were analysed in the Orbitrap detector with resolution R=70,000 at m/z 400. The 12 most intense peptide ions with charge states ≥2 were sequentially isolated to a target value of 3e6 and fragmented with a normalized collision energy setting of 28% in to the HCD cell. The maximum allowed ion accumulation times were 20ms for full scans and 80ms for MSMS. Acquired raw data obtained by mass spectrometry analysis were analyzed using the MaxQuant (MQ) [83] version 1.6.10.43, and peptide lists were searched against the human Uniprot FASTA database (74470 Entries) with the Andromeda search engine [84]. False discovery rate (FDR) for both protein and peptide identifications was set to a maximum of 1% with enzyme specificity set to Trypsin/P. A maximum of 2 missed cleavages was allowed, and the minimum peptide length was fixed at 7 amino acids and Carbamidomethylation of Cysteine was specified as a fixed modification. Peptides were identified with an initial precursor mass deviation of 7 ppm and a fragment mass deviation of 20 ppm. For label-free protein quantitation (LFQ), we required a minimum ratio count of 2 [85]. All proteins and peptides matching to the reversed database were filtered out. ProteinGroups.txt table from MQ output was analysed using a homemade R Studio pipeline and a

moderated t-test statistics from an empirical Bayes method was used. In particular, to identify significantly regulated proteins between sample groups a Benjamini–Hochberg FDR correction corresponding to 5% together with a minimal fold change equal to 1 were imposed. Volcano plots were generated in R Studio using R v4.0.3 and ggplot2 v3.3.5 [86].

3.9 Western blot

Total cellular lysates were obtained using the hot lysis method. Briefly, boiling (96 degrees) lysis buffer made of 125 mmol/L Tris HCl pH 6.8 and 2.5% SDS was added to the cells and left for 15 minutes. From 30 µl to 70 µl for a well of a six well plate, according to cells confluency. Samples were scraped, sonicated and pelleted at 14000 rpm for 10 minutes. Separation was done on gradient gels (Invitrogen, Bolt 4-12% Bis-Tris Plus; NW04120) 1.0 mm X 10 well or 1.0 mm X 15 well. Experiments were made with cooling to avoid any possible side effects due to heating. Gels were transferred to nitrocellulose membrane purchased by BioRad (1704158).

3.10 Immunofluorescence experiments with the RUSH system

Cells were seeded on 12mm coverslips. Twenty-four hours after seeding, microscopes slides were transferred in twenty-four-well plates for transfection. Transfection of the Str-KDEL_SBP-EGFP-GPI construct was done in presence of X-tremeGENETM HP DNA Transfection Reagent (Roche). A mixture containing 0,5 µg of DNA, 1 µl of X-tremeGENETM, and 100 µl of Opti-MEM medium was prepared; left a RT for 15 min and then added to cell. Cells were kept in DMEM 10% 0,1µM Avidin during transfection. Forty-eight hours later, cells were washed twice with PBS, followed by 15 minutes at 37°C in DMEM 10%. 40µM of Biotin was added to the medium at specific time points. Coverslips were fixed and stained in 0.1% Triton as described in the immunofluorescence paragraph.

For colocalization analysis ImageJ JACoP plugin was used. Briefly GM130 and GFP channel were opened in ImageJ software. Automatic threshold of

the JACoP plugin was selected and Pearson's coefficient was calculated. The mean of each value is plotted as shown in Figure10.
For live cell imaging cells were seeded on 25 mm coverslips and transfected as already described in this paragraph.

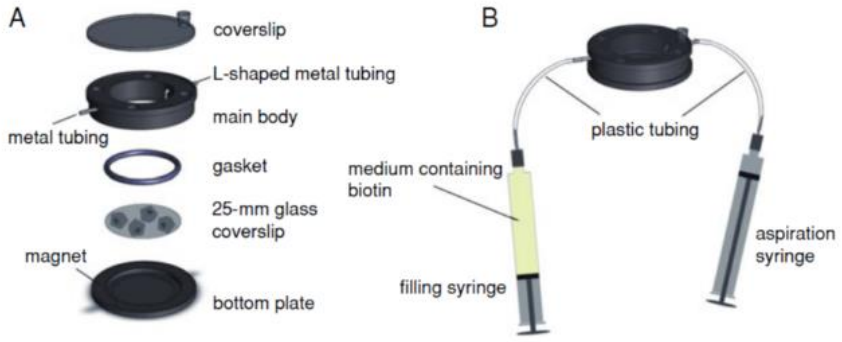

Figure O: Scheme of theL-shaped Chamlide components (A) and assembly (B) for live cell imaging biotin treatment [87]

Coverslips were put on L-shaped Chamlide assembled with tubing and syringes to replace DMEM 10% 0,1mM avidin with Lebovitz medium containing 80µM of Biotin. Imaging was done employing the Inverted Eclipse Ti-E (Nikon)+ Spinning Disk CSU-Xi (Yokogaw Integrated in Metamorph software by Gataca System), objective 60x CFI plan Apo VC, GFP, mCherry filters.

3.11 Protein production and GAP assay

Constructs encoding the GST-tagged proteins were purchased by Addgene or Vector Builder and transformed in BL-21 inducible bacteria. BL-21 expressing the protein of interest were grown overnight at 37°C in 100ml of LB in presence of 100µg/ml ampicillin. The day after bacteria were diluted 1:100 in 1l of LB and grown until OD600=0,6 (approximately for 1 h), then induced with 1mM IPTG for five hours. Bacteria were spun at 3000 rpm for 15 min at 4°C, lysed in Lysis Buffer (50mM TrisHCl, 100mM NaCl pH8, 2mM MgCl2, 0.1% β-mercaptoethanol plus protease inhibitors and 10ug/ml PMSF) and frozen at -20°C. The day after they were thaw, lysozyme was added to a final concentration of 0,02 mg/ml. Bacteria lysate was sonicated (amplitude 30%, 20 seconds followed by 10 seconds pause) and spin at

14000 rpm 1h, at 4°C after Triton-X100 1% supplementation. Proteins supernatants were loaded on 500µl slurry of glutathione magnetic beads (78602, Invitrogen) for 1h at 4°C. Beads were washed three times with Lysis Buffer supplemented with 1% TritonX-100 and three times with Lysis Buffer. Beads were resuspended in 250µl of Lysis Buffer. To quantify the production 10µl and 20µl of slurry beads were taken and eluted by boiling them for 10 min at 96°C in Loading Buffer. These samples were run on gel and stained with Colloidal blue staining together with known quantity of BSA for the estimation of protein concentration. This protocol was slightly modified to produce GST-TBC1D22B and GST-TBC1D22B RQ. In this case, the overnight bacterial colture was diluted 1:100 and 2 liters per construct were prepared. After reaching an OD600 of 1,6, BL-21 bacteria were induced overnight with 0,5mM IPTG. The bacterial pellet was resuspended in 40 ml of lysis buffer and incubated with 500µl of 50% slurry glutathione agarose beads (16100, Pierce) previously washed in Lysis Buffer (50mM TrisHCl, 100mM NaCl pH8, 2mM MgCl2, 0.1% β-mercaptoethanol plus protease inhibitors and 10ug/ml PMSF) as described above. Purified protein on beads were washed with 1ml of GAP Buffer x2 (20 mM HEPES pH 7,5, 150 mM NaCl, 11 mM MgCl2) and resuspended in 100µl GAP Buffer. GST-TBC1D22B and GST-TBC1D22B RQ were cleaved from the GST moiety by adding 1µl of Biotinylated Thrombin (0.5U/µl) for 2 hours at RT. The excess of thrombin was removed using streptavidin-coated magnetic beads (88816, Pierce).

GAP assay was conducted using the Malachite green phosphate assay (MAK-307, Sigma-Aldrich). The reaction is based on the colorimetric quantification of the green complex formed between Malachite Green, molybdate, and free orthophosphate that results measured at 620nm on a spectrophotometer. The GAP assay was done in triplicate using TBC1D22B and GAP buffer as negative control. 200pmol of RABGTPases per point were used adding TBC1D22B with a ratio of 1:20. Loading of GTP on the various RAB GTPases tested was done by incubating the GST-RAB on beads with a 25-molar excess of GTP. To this end, beads carrying the GST-

RAB were washed twice with Loading Buffer (20 mM HEPES pH 7.5, 150 mM NaCl, 5 mM EDTA, 1 mM DTT) then incubated with Loading Buffer supplemented with 60nmol GTP for 20 minutes at 30°C. $MgCl_2$ 1M was added for 5 minutes at 30°C. Beads were recovered on magnetic stand and washed with 1ml GAP buffer x1 (20 mM HEPES pH 7,5, 150 mM NaCl, 11 mM $MgCl_2$). Beads were divided in two Eppendorf, each sample corresponding to 1200 pmol of GST-RAB in a final volume of 100 ml in GAP buffer. Sixty pmol of TBC1D22B or TBC1D22B RQ or GAP buffer as negative control were added and incubated for 8 min at 30°C. Aliquots, 25 ml, in triplicates were taken for the analysis. Malachite green reaction mix was added to the 96 multiwell plate. Color development was read 30 minutes later using the Tecan Spark10M spectrophotometer. The amount of phosphate released was calculated from a standard curve according to manufactures instruction.

3.12 Antibodies

The following antibodies were used: MYC (ab32), HK2 (ab227198), MCT4 (ab234728) and GLUT1 (ab15309) (Abcam); p-EGFR (3777), AKT (2920), p-AKT (9271), RAB6A (9625), RAB35 (9690), RAB5 (3547), HA-tag (3724) SLC1A5 (8057) and GM130 (12480) (Cell Signaling Technology); GAPDH (sc-32233), EGFR (sc-03) HSP90 (sc-13119) (Santa Cruz Biotechnology); TBC1D22B, used in western blot, (HPA027908) and vinculin (V9131) (Sigma); RAB1B (A04589-1) (Boster); TBC1D22B used in immunofluorescence (H00055633-B01P) (Abnova); GM130 (610822), EEA1 (610456/7) and RAB5 (610724) (BD); TGN46 (AHP500) (BioRad); RAB 13 (GTX64803) and RAB18 (GTX64901) (Genetex); Streptavidin-HRP (VK318136) and BODIPY (D3922) (Thermofisher). Rab6-GTP (AG-27B-0004) (AdipoGen). Phalloidin and Streptavidin (S21381) conjugated with the Alexa-555 or Alexa-488 fluorophores and immunofluorescence secondary antibody and DRAQ5 (62251), for nuclei staining, were purchased from Invitrogen.

3.13 Immunofluorescence

BT549 and MDA-MB-468 cells were fixed in PAF 4% for 10 minutes at room temperature. Permeabilization was done in PBS 2% BSA, 0.1% saponin for 30 minutes or with triton 0,1% for 10 minutes at room temperature. Incubation with primary and secondary antibodies was performed in PBS 0.2% BSA, 0.1% saponin for 1 hour, or in BSA 1% after triton permeabilization at RT. Images were acquired using a Leica SP8 AOBS confocal microscope and analyzed with ImageJ. The JACoP plugin was used for the colocalization experiments as previously described.

Immunofluorescence after APEX2 biotinylation:

120000 cells were plated on 12mm coverslips coated with 0,5% Gelatin. The day after cells were treated with 2mM biotin-phenol and H_2O_2 0.2 mM in PBS as previously described in paragraph 3.6. Cells were washed three times with the quencher solution and fixed in PAF 4% for 10 minutes at RT. Permeabilization was performed using triton 0.1% in BSA 1% for 10 minutes at RT. Primary antibody (Myc by Abcam and TGN46 by BioRad) were incubated in BSA 1% (1:200 v/v) for 1 hour at RT, while Strepatividd-555 (Invitrogen) was employed with secondary antibody (Alexa fluor by Invitrogen) for 30 minutes at room temperature (1:1000 v/v in BSA 1%). Coverslips were washed three times in PBS, rinsed in H_2O and mounted with Fluoromount-G.

Lipid Droplet staining and analysis:

Following there are tips according to specific cell lines:

- For lipid droplets growth: incubate cells with 100µM oleic acid (OA) and fatty acid-free BSA (molar ratio 6:1), or with fatty acid-free BSA alone, in complete medium for 24 hours.
- For starvation: incubate cells in RPMI plus 200 µM fatty acid-free BSA overnight.
- For de novo synthesis: Starve cells as above for 25 hours. After four washes with PBS, add 300 µM OA in BSA (6:1 ratio) to the culture

medium (RPMI serum free) for 10 minutes at 37°C to induce lipid droplets formation.

Cells were plated on 12mm coverslips coated with 0,5% Gelatin. Coverslips were washed three times in PBS and fixed in PAF 4% for 10 minutes at RT. Permeabilization was done with 2% BSA, 0.1% Saponine for 30 minutes at RT. Primary antibody (HA by Cell Signaling and GM130 by BD) diluted 1:200 in PBS 0.2% BSA, 0.1%Saponine were incubated for 1 hour at RT. Secondary antibody by Invitrogen, Thermofisher (Alexa-fluor diluted 1:400, BODIPY 2µg/ml starting from a stock solution of 1mg/ml, corresponding to 3.8mM in DMSO) in PBS 0.2% BSA, 0.1% Saponine were incubated for 30 minutes at RT. Coverslips were washed three times in PBS, rinsed in H_2O and mounted with Fluoromount-G.

Z-stacks were acquired using a Leica SP8 AOBS confocal microscope. 8 slides with a depth of 2µm per each image were taken and merged for following analysis.

BODIPY channel merged Z-stacks were opened in ImageJ software. The image was transformed in 8Bit. Brightness and contrast were adjusted according to specific condition. Automatic threshold was imported in dark background mode. Bigger spots were separated employing the Watershed filter. Each LD was quantified analysing particles. The total LD area was divided on the number of cells and the mean was plotted as in figure 4.

3.14 Statistical Analysis

Unless otherwise stated, statistical analysis was performed employing the T-test.

4. Aim

The aim of this PhD project was to identify proteins, among the RabGAP family members, whose expression is altered in breast cancers. The study of their role in the metabolic alteration of these tumors was also linked to demonstrated prognostic value.

5. Results

5.1. Screening for RabGAP proteins that control glycolysis

To understand the involvement of RabGAP in cellular metabolism and more specifically in glycolysis, we individually silenced the forty-five RabGAP members in the Triple negative breast cancer cell lines MDA-MB-468. A non-targeting silencing oligo was used as negative control. Intracellular lactate concentration was measured as readout of glycolysis. L-lactate is known to be responsible of the acidification of the medium since it is secreted in the extracellular environment. This secretion depends on the activity of the lactate transporters MCT1 and MCT4. Since the role of RabGAP in trafficking of the lactate transporter is unknown, we choose to measure the intracellular lactate concentration to avoid any possible involvement of RabGAP in its secretion. The measured concentration of lactate was normalized over the number of cells in each sample to obtain the concentration in pmoles per cell [data for MDA-MB-468 are shown in Fig.1]. The experiment was repeated three times to achieve statistical significance. The concentration of lactate in cells silenced with control oligo was found to be 0.21644 pmol/cells and it was used to setup the threshold. Depletion of four RabGAPs resulted in increased L-lactate concentration more than 30% compared to control: TBC1D4, TBC1D16, TBC1D2B, RABGAP1L. Among them, TBC1D4 has been previously shown to inhibit translocation of the glucose transporter GLUT4 to the plasma membrane, thus it can be considered a positive control in our experiments. Conversely, twelve RabGAPs showed a reduction of L-lactate concentration upon silencing of at least 30% compared to the control: TBC1D7, TBC1D22A, TBC1D29, TBC1D26, EVI5, TBC1D25, TBC1D22B, TBC1D31, TBC1D3B, TBC1D3F, SGSM1 and USP6NL [Fig.1]. Their ability to impair glycolysis when depleted, suggests that these molecules might promote glycolysis elevation in cancer. Along this line, USP6NL was previously found to control glycolysis elevation in Triple Negative breast cancer cells thus working as a positive control [48].

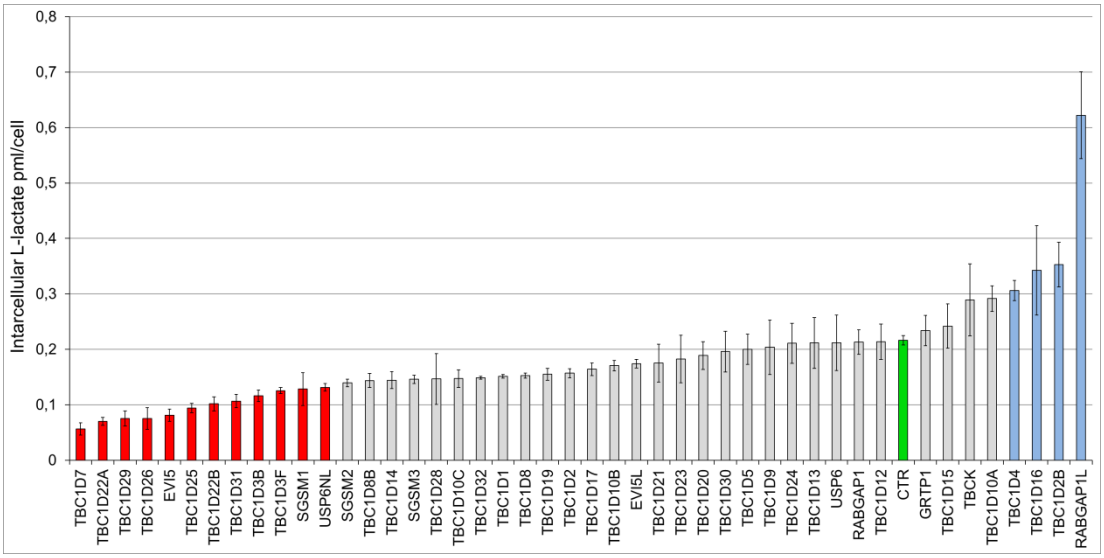

Figure 1. Screening for glycolysis modifiers among the RabGAP proteins

The expression of the forty-five RabGAP proteins (indicated on bottom) was individually knocked down in the MDA-MB-468 cell line by transient siRNA of a pool of four oligos for each RabGAP purchased from Dharmacon or with non-targeting siRNA oligo as negative control (CTR). Intracellular lactate was extracted from cells and measured with the Promega Lactate-Glo kit as described in Methods. The bar graph shows the amount of intracellular lactate (pmol/cell). Mean values ± sem (n=5), from three independent experiment. In red there the RabGAPs whose silencing decrease lactate amount of at least 30% are shown while in blue are those increasing its concentration of at least 30% compared to control levels (CTR, in green).

5.2. Prognostic value of *RabGAP* genes in breast cancer patients

We investigated alterations in the expression levels of the forty-five genes encoding the RabGAP proteins in breast cancer patients correlating this information with tumor subtypes and survival. To this end, we employed the METABRIC dataset, available at https://www.cbioportal.org, that collects gene expression data and clinical-pathological parameters from around 2000 breast cancer patients with a follow up of 20 years [48], [88] . In breast cancer, a long follow up is required to fully understand the predictive value

of genes because a large fraction of patients, typically Luminal patients, remain at risk of relapse for very long times, even more then 15 years [89] . By evaluating the mRNA expression data of the RabGAP genes in 1980 breast cancer patients we found that four, *TBC1D31, TBC1D7, TBC1D22B,* and *USP6NL* were highly expressed in breast tumors correlating with worse prognosis in univariate and multivariate analysis (HR and HR* respectively) [Fig.2]. In breast cancer, the availability of several prognostic parameters allows to perform multivariate analyses that can determine whether the gene alteration under investigation is an independent predictor of outcome by comparing its predictive value with five known prognostic parameters: Lymph node status, Hormonal status (ER and PgR), HER2 amplification, Tumor grade and size [90]. Among four RabGAP genes identified, TBC1D7 and USP6NL were expressed at higher levels in the TNBC subtype while the levels of expression of TBC1D22B were raising along with the increased aggressiveness of the subtypes [Fig. 2]. The higher number of cases carrying overexpression of *TBC1D22B* was found in the Luminal subtype.

We crossed these results with data from the glycolytic screening described in paragraph 5.1 finding that the functional ablation of all these four RabGAPs was reducing the intracellular production of lactate. Taken together, these findings suggest that these four RabGAPs might be required for glycolysis elevation in breast cancer and this function might increase tumor aggressiveness thus providing a causative role for the elevated expression of these molecule in the more aggressive breast tumors showing reduced survival.

Among the four RabGAPs identified, the role of USP6NL in glycolysis in breast cancer was previously addressed (described in paragraph 2.3) finding that, by restraining the endocytosis of the EGFR, it causes prolonged AKT activation and GLUT1 accumulation to the plasma membrane with consequent increase in glucose uptake. Moreover, USP6NL has been shown to determine glycolysis addiction in breast cancer cells since starvation from glucose impairs the viability of breast cancer cell lines that

express high levels of USP6NL and this sensitivity is abrogated upon silencing of USP6NL [48].

Concerning TBC1D31 and TBC1D7, both these two RabGAPs carry a GAP domain that is thought to be defective because it lacks the catalytic residues. Therefore, their involvement in the regulation of breast cancer cell metabolism should be, at least in principle, independent from direct trafficking-mediated events.

Instead, TBC1D22B is a functional RabGAP still uncharacterized. Based on this, we choose to concentrate our efforts in understanding the biological function of TBC1D22B and its role in breast cancer cell metabolism. In the following paragraph we will illustrate what we learned so far about the function of TBC1D22B in the regulation of membrane trafficking and cell metabolism.

A

Gene	METABRIC mRNA EXPRESSION/SURVIVAL in 1909 patients					METABOLIC SCREENINGS
	mRNA Levels Nor vs Tumors	Univariate		Multivariate		Molecular Subtype	DOWN >30% reduction
		HR	P value	HR *	P value		L-lactate
TBC1D31	**UP**	1,69	<0.0001	**1,343**	**0,0018**		**DOWN**
USP6NL	**UP**	1,607	<0.0001	**1,218**	**0,039**	TNBC	**DOWN**
TBC1D7	**UP**	1,438	<0.0001	**1,69**	**0,009**	TNBC	**DOWN**
TBC1D22B	**UP**	1,416	<0.0001	**1,274**	**0,004**	Luminal	**DOWN**
TBC1D26	FC N/T 0.98	1,209	0,019	1,207	0,02		
RabGAP1	DOWN	1,118	0,04	1,243	0,008		

B

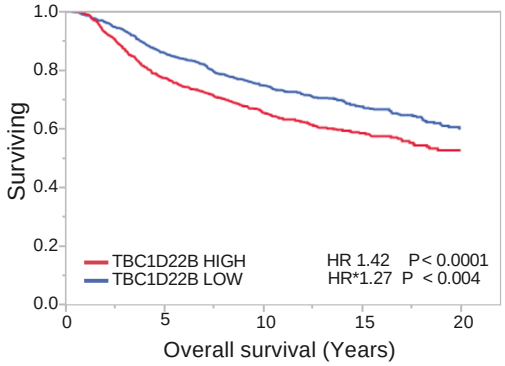

C

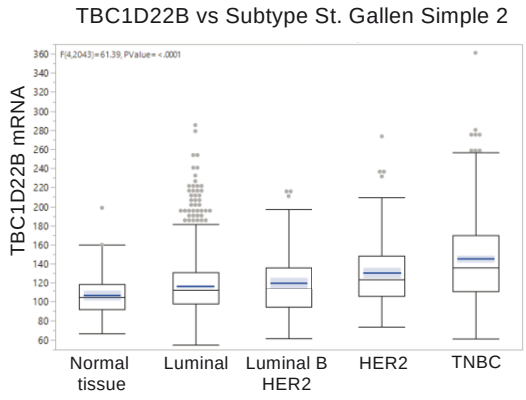

Figure 2. METABRIC analysis

A) The table shows the correlation between RabGAPs expression with prognosis and tumor subtype. The hazard ratio relative to the mRNA overexpression is reported in univariate analysis (HR) and multivariable

analysis (HR*). Association with molecular subtypes is annotated; performance in the glycolytic screening is shown in the last column.
B) Correlation between TBC1D22B mRNA level and tumors subtype according to St. Gallen classification.
C) Kaplan-Meier showing the correlation between high level of TBC1D22B and the survival rate.

5.3. Investigation of the TBC1D22B in energy metabolism

To address the metabolic function of TBC1D22B we investigated the effects of its knock down on the cell energy metabolism using the Seahorse technology. To this end, TBC1D22B was silenced in the triple negative breast cancer cell line MDA-MB-468 and glycolysis and mitochondrial respiration were evaluated in the silenced cells by measuring respectively the Extracellular Acidification Rate (ECAR) and the Oxygen consumption Rate (OCR). In the EACR analysis, glucose was added to start glycolysis, followed by treatment with Oligomycin, which inhibits mitochondrial oxidative phosphorylation allowing the measurements of the maximal glycolytic capacity, and with the Glucose analogue 2-Deoxy-D-glucose (2-DG) which cannot be processed by glycolysis enabling measurement of the glycolytic reserve (which results from the maximal glycolytic capacity subtracted of the basal glycolytic rate).

The OCR analysis started by the evaluation of basal respiration (Oxygen consumption used to produce ATP). Oligomycin was injected to inhibit ATP synthase resulting in a decreasing mitochondrial respiration, followed by Carbonyl cyanide-4 (trifluoromethoxy) phenylhydrazone (FCCP) which cause the collapse of proton gradient resulting in maximum oxygen consumption. The FCCP-stimulated OCR can then be used to calculate spare respiratory capacity, defined as the difference between maximal respiration and basal respiration.

Lastly Rotenone and Antimycin A were injected to inhibit complex I and III, shutting down mitochondrial respiration enabling us to calculate the nonmitochondrial activity (Oxygen consumption that persists due to a subset of cellular enzymes).

We observed that silencing the expression of TBC1D22B reduced glycolysis and the glycolytic capacity, also confirming the results generated for TBC1D22B in the RabGAP screening. Furthermore, reduced basal respiration and proton leak indicates the depletion of TBC1D22B also affect mitochondrial functions [Fig. 3A-D]. These results point to a positive function for TBC1D22B in the cell energy metabolism. To investigate if the role of the RabGAP on cell metabolism was due to an impairment of cell viability we performed a cell proliferation assay on TBC1D22B knockdown MDA-MB-468 cells [Fig. 3E]. Cells were plated and monitored every other day for a maximum of three days. Results obtained in silenced cells were compared to control condition, showing no significant differences [Fig. 3E]. It is possible to conclude that metabolic alteration due to TBC1D22B activity are not related to cell viability.

Moreover, nutrient transporter regulation was evaluated in silencing condition in the same cell line, MDA-MB-468. The levels of glucose, monocarboxylate and glutamine transporter; GLUT1, MCT4 and SLC1A5 respectively, were evaluated in western blot analysis. Again, no significant differences were revealed comparing TBC1D22B knock-down with control [Fig. 3F]. Only the total amount of these proteins was analyzed, leaving the possibility that the RabGAP of interest affects cell surface expression of transporters. However, the amount of internalized glucose was not found to be altered in cells lacking TBC1D22B [Fig. 3G]. Together, these results suggest that the effect of TBC1D22B silencing on intracellular lactate concentration are likely independent from alteration of glucose metabolism. Previous studies demonstrated that glutamine can support lactate production via re-conversion of malate to pyruvate [91]. Hence, TBC1D22B role in glutamine metabolism might be worth investigating.

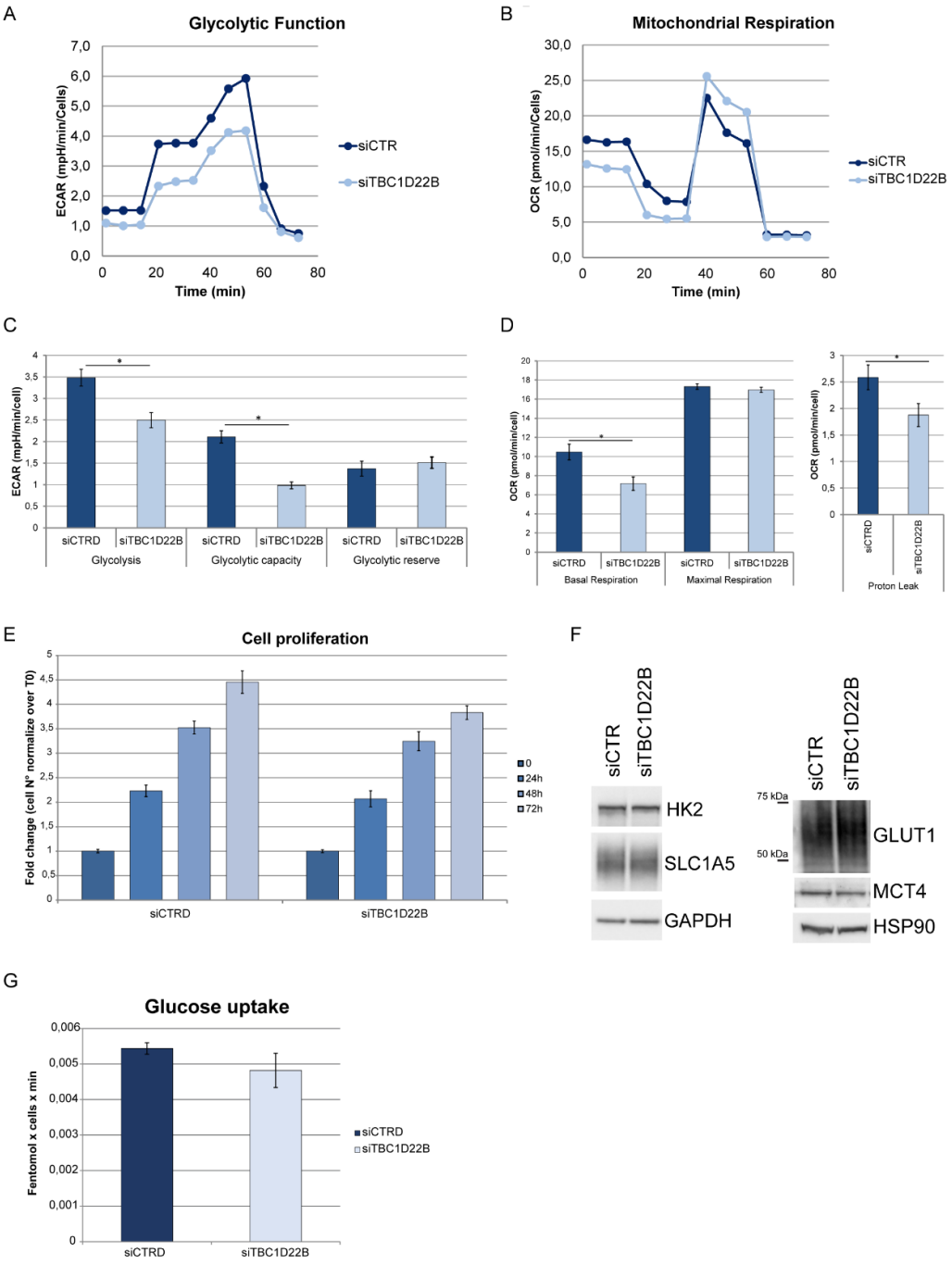

Figure 3. glycolysis and mitochondrial respiration in cells depleted of TBC1D22B

A) Representative curve of ECAR levels and OCR (B) from 3 independent experiments in MDA-MB-468 cells silenced as in the legend. Each point is the mean ± s.e. of six technical replicates.

C-D) Histograms show the single parameter (indicated on bottom) and are the mean of three independent experiments ± s.e. (18 technical replicates) p value <0.01.
E) Histograms represent cell viability fold change over time point indicated in the legend of MDA-MB-468 cells silenced as reported on bottom. ± s.e. N=4
F) Total cellular lysates from MDA-MB-468 cells silenced with CTR siRNA or TBC1D22B siRNA, were immunoblotted for glutamine/glucose transporters as indicated on the right.
G) Histograms show the amount of glucose uptake normalized over cell number in MDA-MB-468 cells silenced as in the legend. ± s.d. N=1

5.4. TBC1D22B promotes lipid storage in a GAP dependent manner

The elevation of glycolysis in cancer cell provides intermediates to feed anabolic pathways such as the pentose-phosphate pathway, the hexosamine pathway, glycerol biosynthesis, and serine–glycine–one-carbon metabolism [16]. Moreover, glucose can be employed in the Tricarboxylic Acid Cycle to produce citrate, which exit the mitochondria to be used in the cytoplasm for fatty acid synthesis [92]. Because de novo lipogenesis is a distinct tract of aggressive breast cancer [14], we tested if TBC1D22B participates to lipid production and storage.

To address whether this function might be linked to the regulation of membrane trafficking, we generated a GAP-defective TBC1D22B mutant by mutagenizing the catalytic residues arginine at position 274 and glutamine at position 309 to alanine. These two residues have been selected for mutagenesis based on the alignment of TBC1D22B with other RabGAPs for which the catalytic residues have been identified and experimentally validated. We generated stable cell populations in the BT549 cell line overexpressing TBC1D22B or the GAP-defective mutant by infecting the BT549 cells with lentiviral vectors carrying HA-tagged TBC1D22B or

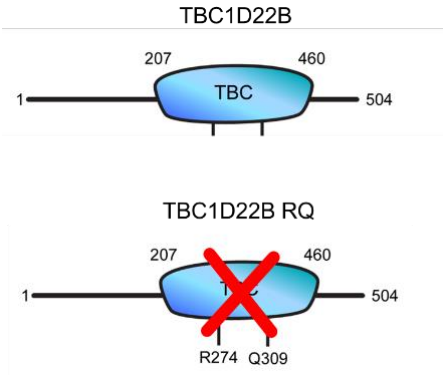

TBC1D22B RQ. Stable cell populations were established by puromycin selection.

The effect of overexpression of wild type and mutant TBC1D22B on the formation of Lipid Droplets was evaluated by staining the cells with BODIPY a fluorescent marker of neutral lipids showing that increased amount of TBC1D22B resulted in Lipid increased Droplets size, up to 10 times compared to the negative control [Fig. 4]. Conversely, abrogation of the TBC1D22B GAP activity did not exert a comparable effect [Fig. 4] indicating that the function of TBC1D22B in lipid droplets accumulation is GAP-dependent.

These initial findings suggest possible functions for TBC1D22B in energy metabolism and lipid storage that are currently under investigation by testing whether lipid droplets accumulate because of increased nutrient uptake, upregulation of de novo lipogenesis enzymes or by reduced lipophagy.

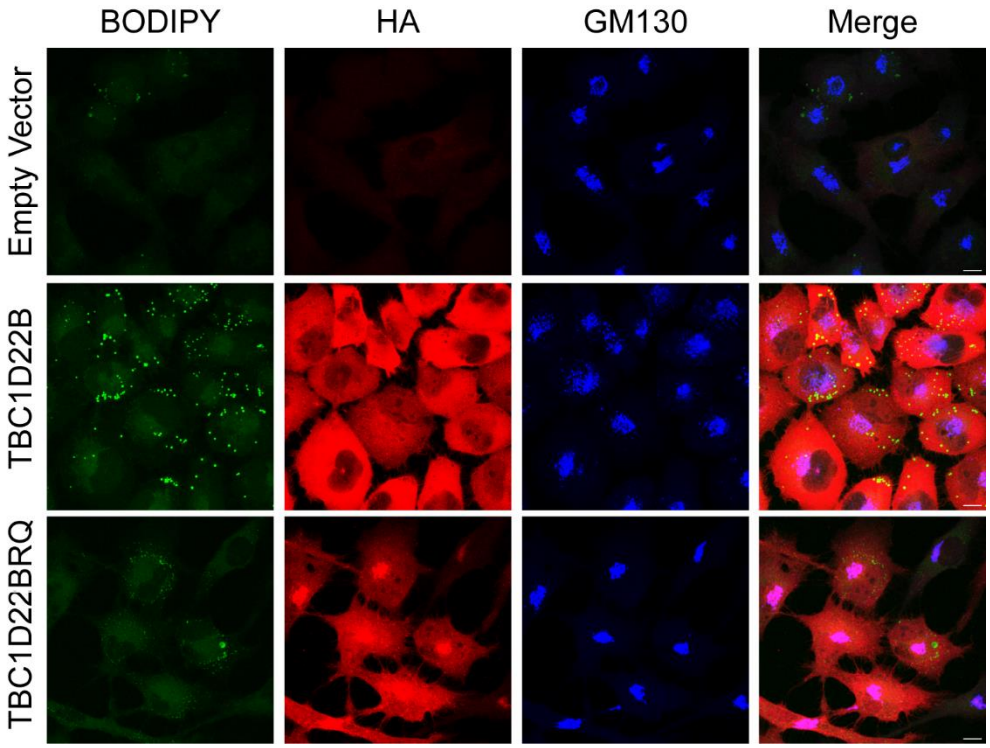

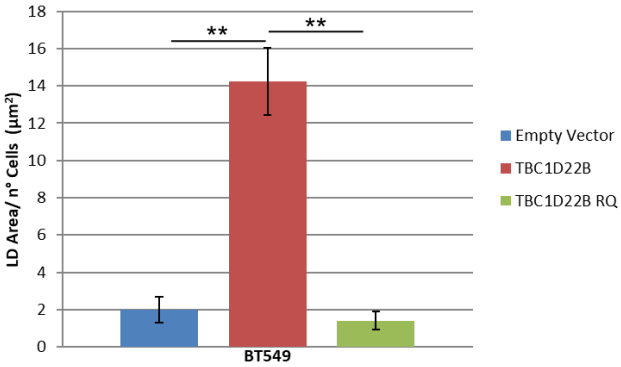

Figure 4. Increased amount of TBC1D22B causes accumulation of Lipid droplets in a GAP-dependent manner

Representative merged Z-stack confocal images of BT549 cells empty vector, or overexpressing TBC1D22B or TBC1D22BRQ (indicated on the left). Expression of TBC1D22B or TBC1D22BRQ is revealed by staining with an anti-HA antibody (Cell signaling 3724, in red). The Golgi is visualized by staining with the anti-GM130 antibody (BD, 610822, in blue), while Lipid Droplets are shown by BODIPY staining (Thermofisher, D3922, in green). Quantification of Lipid Droplets area was done using ImageJ as previously described. N=1, n° of cells= 100. The bar corresponds to 10µm.

5.5. Identification of the TBC1D22B protein interacting network by proximity biotinylation

To gain insights on the function of TBC1D22B we isolated its interacting protein network using the proximity biotinylation technique. The TBC1D22B RQ mutant was also employed to test whether abrogation of the enzymatic activity would alter the composition of the interactome. First, we designed the constructs. We fused the APEX2 enzymatic domain in frame with the N-terminus of TBC1D22B and TBC1D22B RQ in the lentiviral pLV backbone. A myc tag was inserted at the N-terminus of APEX2, while the HA tag was added to the N-terminus of the TBC construct (between the APEX2 and TBC1D22B sequences). This has been done to separate APEX2 from the TBC protein facilitating the biotinylating activity of the resulting chimera. Next, we established stable cell population by infecting BT549 cells with these lentiviral constructs followed by puromycin selection and the expression and localization of the constructs was determined by

immunofluorescence and western blot analysis [Fig. 5A-C]. TBC1D22B a Golgi protein showed co-localization with the trans-Golgi marker TGN46 [Fig.5A]. Both the APEX2-TBC1D22B wild type and mutant chimeras were found to similarly accumulate at the Golgi apparatus [Fig.5C]. Moreover, we tested the specificity of the biotinylation activity of the two chimeras at the subcellular levels by performing biotinylation followed by staining with fluorescent-tagged streptavidin [Fig. 5C]. We found that the biotinylation activity, revealed by streptavidin staining was higher at the Golgi apparatus with little diffuse staining in the cytoplasm [Fig.5C]. One of the major limitations of the proximity biotinylation technique is the aspecific biotinylation of proteins which may occur upon ectopic expression of the APEX-fusion proteins. Despite our results indicate that the majority of the biotinylation activity is concentrated at the proper location, the Golgi apparatus, to overcome the limitation of aspecific biotin tagging by the APEX2 constructs, we employed several negative controls and we set up stringent conditions in the pull-down assay. We started from published methods and adapted them to our cells and constructs resulting in an improved protocol. The major improvements are detailed here below:

- As for the negative controls, we performed the pull down from cells carrying the empty vector or the chimeras incubated in presence of hydrogen peroxide but without biotin-phenol.
- We set up the biotinylating conditions by performing titration experiments in which we treated cells with different amount of biotin-phenol and H_2O_2 to identify the optimal concentration of both component (the final conditions are in Figure 6, the intermediate steps of the setting up procedure are not shown). We found that optimal biotinylation in the BT549 cells was obtained incubating cells with 2mM biotin-phenol followed by treatment with 0,2mM H_2O_2 for 1 min.
- One major problem encountered in this type of experiment is the high amount of biotinylation that is obtained also in the negative

(empty vector) control. We found that increasing the denaturing conditions in the lysis buffer, used to extract the biotinylated proteins from cells, strongly reduced the recovery of proteins with low or non-specific levels of biotinylation.

- Stringency of the washing steps was increased as described in the Method section.
- Four replicates per condition were analyzed to achieve statistical significance.

Figure 6 shows a typical pull-down experiment. Samples were run on gel and stained with Colloidal blue to reveal the total amount of proteins in the various conditions. The stringent conditions adopted and described above, allowed us to obtain negative control pull down samples carrying very low amounts of biotinylated proteins [Fig.6A]. The streptavidin HRP western blot reveals efficient pull down of the biotinylated protein in the APEX2-TBC1D22B and APEX2-TBC1D22B RQ samples only in the samples obtained from cells that were incubated with both biotin-phenol and H_2O_2 [Fig.6B]. Samples corresponding to those shown in Figure 6 were trypsin digested and the peptides generated were analyzed by liquid chromatography/mass spectrometry (LC/MS). Each sample was run twice generating eight LC-MS runs per condition. Shot gun mass spectrometry, protein identification and statistical analyses were performed by our collaborators Alessandro Cuomo and Fabio Bedin at the European Institute of Oncology in Milan.

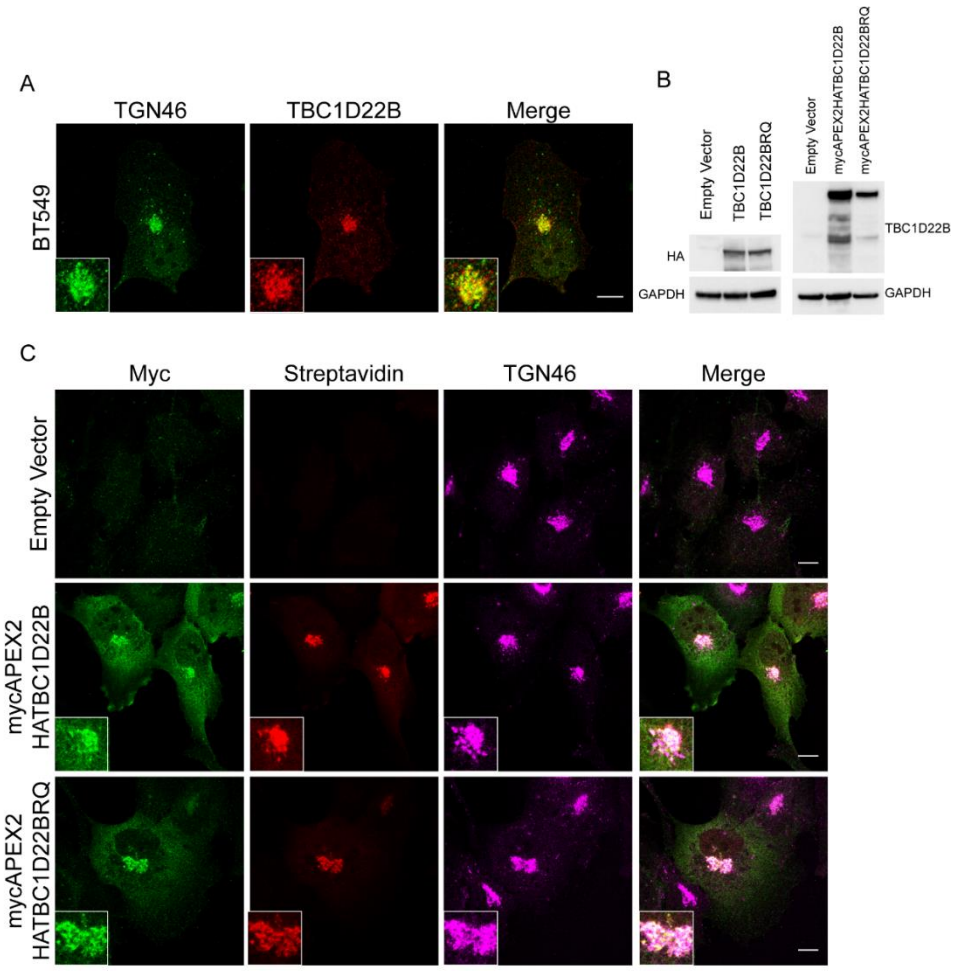

Figure 5. Localization and activity of APEX2-TBC1D22B and its mutant

A) Localization of endogenous TBC1D22B to the Golgi. Confocal image of BT549 cell stained with an antibody against the Golgi TGN-46 (BioRad AHP500, in green) and anti-TBC1D22B (Abnova, H00055633-B01P, in red). Colocalization is shown by yellow staining in the merge. Bar, 10 mm.
B) Total cellular lysates from BT549 cells stably expressing the empty vector, TBC1D22B or TBC1D22BRQ were immunoblotted as indicated
C) Confocal images of BT549 cells stably expressing the empty vector, TBC1D22B or TBC1D22BRQ that underwent biotinylation followed by fixation and staining with anti-myc antibody (Abcam ab32, in green), Streptavidin, Alexa Fluor 555 conjugate (Invitrogen, S21381in red) and anti-TGN46 antibody (in magenta). Colocalization results in white staining in the merge. Bar, 10 mm.

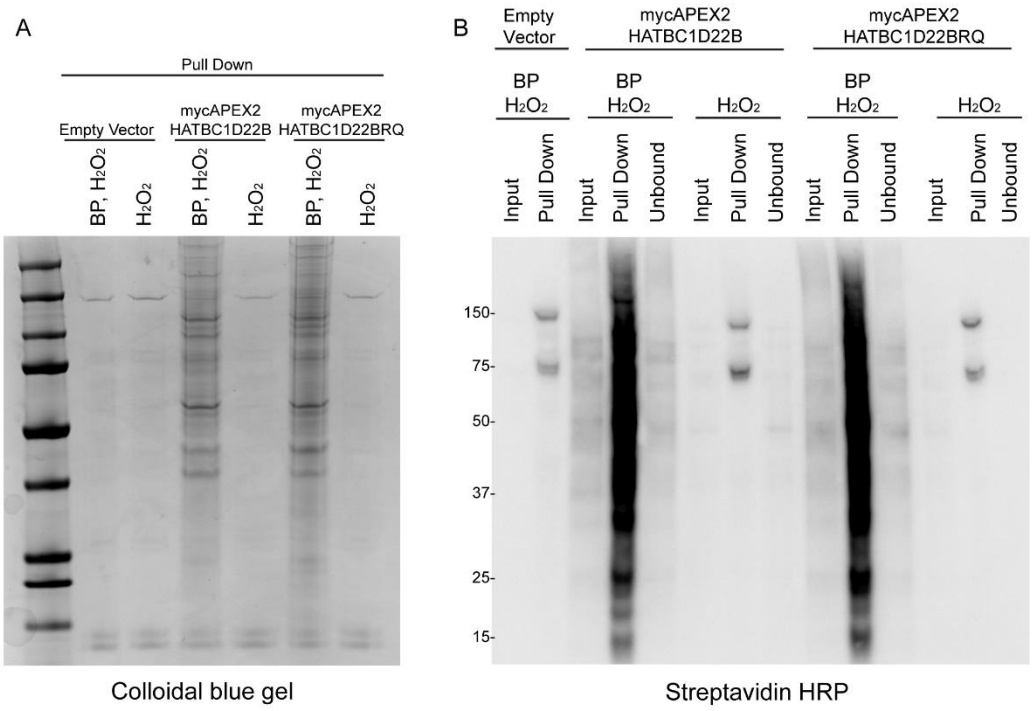

Figure 6. Streptavidin pulldown assay of proteins biotinylated by APEX2-TBC1D22B and APEX2-TBC1D22BRQ

A) Colloidal blue gel and B) Streptavidin-HRP Western Blot of samples from BT549 cells expressing empty vector, APEX2-TBC1D22B or APEX2-TBC1D22BRQ indicated on top.

A) In the Colloidal blue gel, BP, H_2O_2 indicate the pull-down samples obtained from cells (indicated on top) that were incubated with both biotin-phenol and H_2O_2. Pull down samples indicated with H_2O_2 were obtained from cells treated with H_2O_2 without prior incubation with biotin-phenol. The pull down corresponds to 1/3 of the pull down that was digested and analyzed by mass spectrometry (equivalent to pull down of 1,5 mg of total biotinylated lysates).

B) Streptavidin-HRP Western Blot of samples from the cells treated as indicated on top. Inputs corresponds to 5 mg of total cellular lysates. The samples marked as unbound correspond to the lysates after streptavidin pull down (the same volume as the inputs has been run).

We identified two categories of putative interacting proteins. The first category corresponds to the proteins that were significantly enriched in the pulldown from cells expressing APEX2-TBC1D22B compared to the empty vector after applying a false discovery rate < 5% with a p value adjusted (Benjamini Hochberg) <0.05. They were 176 proteins shown in the Volcano Plot of Fig. 7A. The second category was made by proteins that were detected in at least three pull down from cells expressing APEX2-TBC1D22B and absent or detected only in one sample out of four in the pull down from control cells, they were 1572 proteins, that we defined “unique” for the TBC1D22B interactome.

We analyzed all the significantly biotinylated proteins identified for gene ontology (GO) term enrichment, focusing on cellular components and biological processes categories. We found that, the term showing the highest statistical significance (1,6E-49) was "focal adhesion” followed by other highly significant and related terms, “Golgi vesicle transport”, “integrin complex” and “Endoplasmic Reticulum exit site” and “cell-cell junction” [Fig. 7B]. Looking at the proteins identified in the TBC1D22B proximity interactome that belong to these terms, we noticed several integrin receptors: integrin β1, integrin α2, integrin α3 and integrin α6. These analyses suggest a function for TBC1D22B in Golgi trafficking of integrin receptors.

Since TBC1D22B is a RabGAP protein, we looked for RAB GTPases in the list of proteins biotinylated by the APEX2-TBC1D22B chimera. We found eleven RAB GTPases that mostly regulate Golgi and endosomal trafficking pathways: RAB6A, RAB7A, RAB10, RAB13, RAB18, RAB1B, RAB21, RAB34, RAB35, RAB5C and RAB8A [52], [53]. Moreover, other RabGAP proteins were also present in the TBC1D22B proximity interactome: RABGAP1 (also known as GapCenA), RAB3GAP2 and TBC1D15. TBC1D15 is a GAP for RAB7A suggesting that some of the RABs identified might not be direct targets of TBC1D22B, but rather of other TBC1D22B-interacting RabGAPs, in line with previous finding showing that another

RabGAP, RUTBC2, works at the same time as a RAB9A Effector and a GTPase-activating for RAB36 [41].

Next, we compared the proximity interactome of TBC1D22B with the one isolated from cells expressing the GAP-deficient mutant, TBC1D22B RQ finding that 107 proteins were differently enriched in the two interactomes [Fig.8A].

By performing a functional analysis on the proteins that were differentially associate with the wild type or the mutant interactomes, we found that the integrins receptors ITGA2 and ITGA3 were lost in the mutant interactome [Fig. 8B]. Conversely proteins associated with Golgi-derived vesicles were abundant in the mutant interactome but not in the wild type [Fig. 8C]. These results are compatible with the hypothesis that TBC1D22B inhibits integrin Golgi trafficking.

We noticed that all the RABs identified in the TBC1D22B proximity interactome were also present in the interactome generated by the mutant. We envision two possible explanations:

i) Since the mutant localizes as the wild type, possibly in the same membrane microdomains, it might biotinylate the neighboring proteins as for the wild type. Thus, even if it does not bind to the RABs, they are close enough to be biotinylated by its APEX2-chimera to an extent similar to the one of the wild types.

ii) Binding to the RABs occurs outside the GAP domain and is not abrogated by the RQ mutations.

As a proof of principle, we tested the GAP activity of TBC1D22B on some selected RABs (RAB1B, RAB6A, RAB13 and RAB35) using the Malachite green phosphate assay. The GST-fusion version of the four RABGTPase purchased by Addgene or VectorBuilder were produced in the BL-21 bacteria and purified and quantified on Colloidal blue stained gels [Fig.9A]. GST-TBC1D22B was produced, purified and cleaved from the GST mojety with thrombin. We employed a biotinylated version of thrombin that was subsequently removed by incubating with streptavidin beads. The GST-

RAB were loaded on beads with an excess of GTP, and the unbound nucleotide was removed by subsequent washes in GAP buffer.

The GAP assay was conducted by incubating 1200 pmol of each GTP-loaded GST-RAB with 60 pmol of TBC1D22B in a ratio 20:1 for 8 min at 30°C or with GAP buffer as negative control, the measurements were done on technical triplicates and the experiment was independently repeated three times [Fig. 9B]. We found that TBC1D22B can stimulate GTP hydrolysis on all the RABs tested. So, to test for the specificity of the activity detected we repeated the GAP assays on RAB1B using the GAP-defective mutant as control [Fig. 9D]. The quantification of GST-RAB1B as well as purified TBC1D22B and TBC1D22BRQ is shown in Figure 9C. The addition of TBC1D22B RQ caused a release of GTP similar to the negative control indicating that TBC1D22B is a GAP for RAB1B at least in vitro.

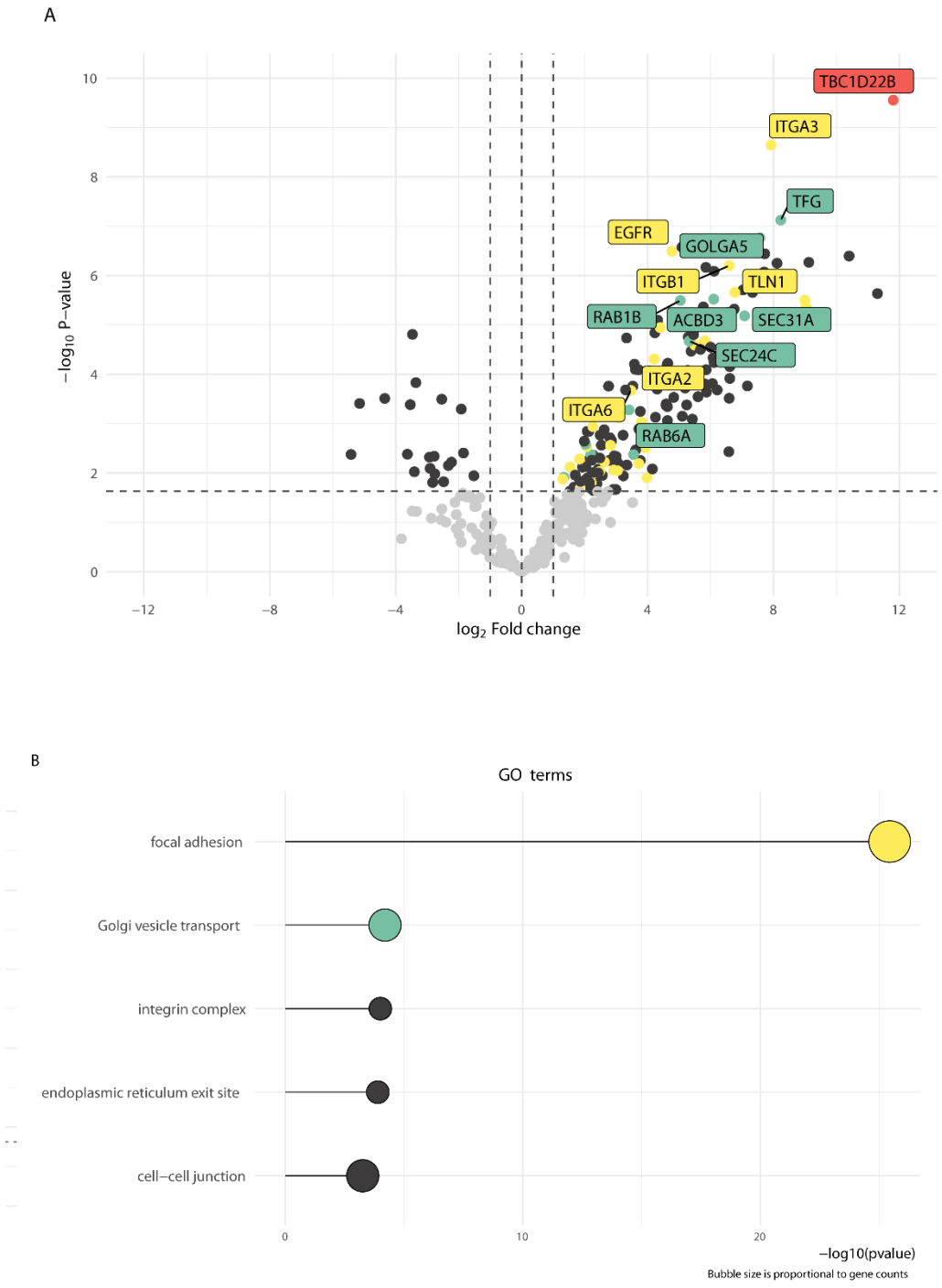

Figure 7. The TBC1D22B vs Empty vector interactome revealed by proximity biotinylation

A) Volcano plot showing proteins significantly biotinylated by Empty Vector (left) or TBC1D22B (right). TBC1D22B is highlighted in red. Proteins belonging to focal adhesions are shown in yellow, those that are part of the

ER-Golgi system are in green. Some selected proteins of the two compartments are labelled.
B) Bubble plot showing representative categories of the Gene ontology (GO) terms significantly enriched in the TBC1D22B proximity interactome. Bubble size is proportional to gene count.

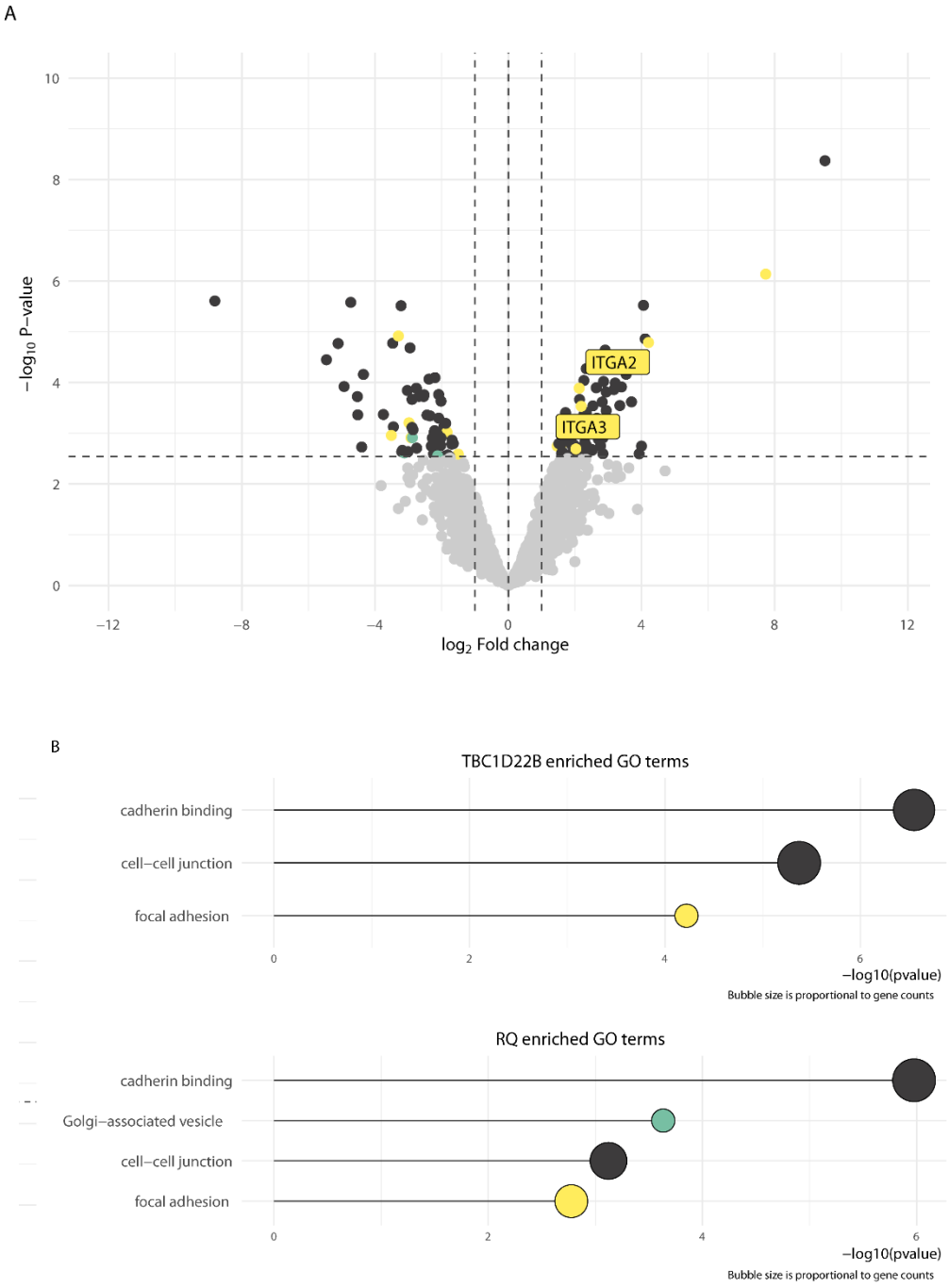

Figure 8. TBC1D22B vs TBC1D22BRQ interacting network analysis

A) Volcano plot of proteins significantly biotinylated by TBC1D22B (right) and the GAP-defective TBC1D22BRQ mutant (left). Highlighted in yellow and green there are the proteins belonging to focal adhesion and ER-Golgi system respectively.

B) Bubble plot of GO terms significantly enriched in the TBC1D22B (top) and TBC1D22B RQ (bottom) proximity interactomes. The “focal adhesion” category highlighted in yellow, was found in both conditions, while integrins were found only in the TBC1D22B interactome. Bubble size correspond to gene count.

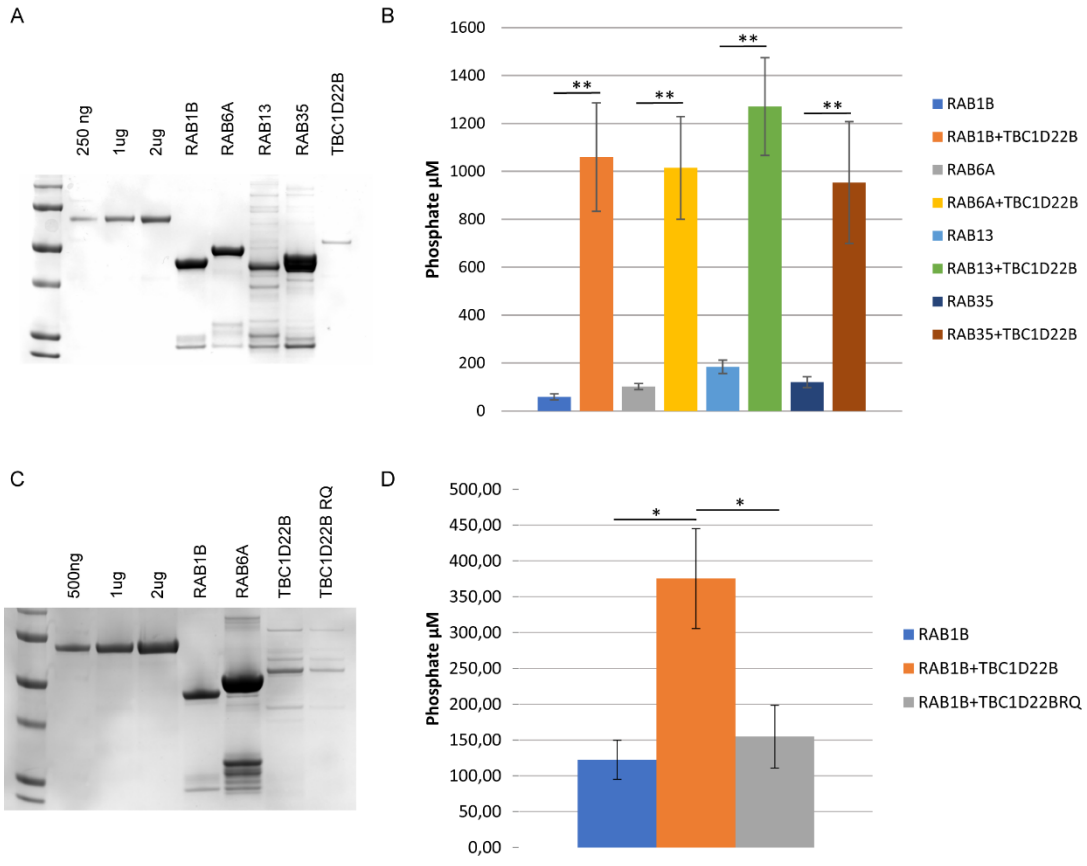

Figure 9. TBC1D22B GAP activity

A) Colloidal Blue gel showing 1 ml of the indicated GST-RABs and 5 ml of TBC1D22B (after cleavage from the GST mojety).

B) GAP assays. 1200 pmol of each GST-RAB (indicated on bottom) were incubated with 60 pmol of TBC1D22B (ratio 20:1) for 8 min at 30 °C or with buffer alone as indicated in the legend. The bar graph shows the phosphate

released quantified by malachite green colorimetric reaction n=3 ± s.e. **p value<0.005, *p value<0.01.
C) Colloidal Blue gel showing 3 ml of the indicated GST-RABs and 5 ml of TBC1D22B and TBC1D22BRQ (after cleavage from the GST mojety).
D) GAP assay. 1220 pmol of GTP-loaded GST-RAB1B were incubated with buffer alone or with 60 pmol of TBC1D22B or 60 pmol of TBC1D22BRQ for 8 min at 30°C. The bar graph shows the phosphate released quantified by malachite green colorimetric reaction n=3 ± s.e. *p value<0.01.

5.6. Role of TBC1D22B in the anterograde transport

Based on the localization of TBC1D22B to the Golgi compartment and on the high number of proteins involved in Golgi transport found in the TBC1D22B interactome, we tested the effect of TBC1D22B on Golgi trafficking focusing on the anterograde ER to the Golgi transport.

To this end, we employed the Retention Using Selective Hooks (RUSH) System [87], [93]. The RUSH system is a two-state assay based on a hook fused to streptavidin and a reporter fused to the streptavidin-binding peptide (SBP) and fluorescently tagged with the Green Fluorescent Protein (GFP) [87], [93]. The hook employed in this system is an ER resident protein or correspond to a protein sequence that targets to the ER. The report is a molecule, usually a receptor, that travels from the ER to the Golgi and, from the Golgi to the plasma membrane. Binding of the reporter to the hook retains it in the ER preventing it from moving to the Golgi and the cell surface. Addition of biotin, by competing with the streptavidin binding peptide, release the reporter from the hook enabling it to travel to the Golgi and then to the plasma membrane. The RUSH system, therefore, is an assay designed to study the anterograde ER to Golgi and Golgi to plasma membrane transport. To test whether TBC1D22B participates to the anterograde transport route, we generated BT549 cell populations stably expressing TBC1D22B, the GAP-deficient mutant TBC1D22B RQ, or the empty vector upon infection with lentiviral vectors. Cells were transiently transfected with the RUSH construct Str-KDEL_SBP-EGFP_GPI in presence of 1µM avidin to neutralize any possible biotin contamination from

the medium. Two days after transfection, cells were washed with PBS to remove avidin, medium was changed and 40µM of Biotin was added. After Biotin treatment at different time points: 0, 20', 120', cells were fixed and stained with the Golgi marker GM130. Transport from the ER to the Golgi was evaluated by measuring the extent of colocalization between the GFP fluorescence of the RUSH construct and the GM130 marker at each time point, using ImageJ plugin JacoP. In control cells the reporter reached the Golgi apparatus in approximately 20 minutes and after two hours was mostly at the plasma membrane [Fig.10A-B]. Instead, in cell overexpressing TBC1D22B, 20 minutes were not sufficient to reach to the Golgi, however, two hours later the Golgi localization was clearly visible. [Fig.10A-B]. Conversely, in the cells overexpressing the GAP-deficient RQ mutant the reporter travelled without any delay from the ER to the Golgi indicating that the GAP activity of TBC1D22B is required to restrain ER to Golgi transport [Fig.10A-B]. Again, the reporter remained for a long time in the Golgi (more than 60 min) showing a delay in reaching the plasma membrane similar to one measured in the cell expressing TBC1D22B wild type [Fig.10A-B]. These latter findings suggest that TBC1D22B controls ER to Golgi translocation by inhibiting the function of some RAB(s) and participates to the delivery of proteins from the Golgi to the plasma membrane in a GAP-independent manner. Alternatively, the delay in plasma membrane delivery exerted by TBC1D22B might result from the previous delay in the ER to Golgi translocation, while the delay caused by the mutant could depend on a neomorphic function of the mutant itself. To confirm the measurements obtained on fixed cells, we repeated these experiments by live cell imaging experiments in the laboratory of Franck Perez, who developed the RUSH system, at the Institute Curie in Paris. To this end, BT549 cells were transiently co-transfected with the RUSH construct Str-KDEL_SBP-EGFP_GPI together with either TBC1D22B tagged with the mCherry or with mCherry-TBC1D22BRQ. Twenty-four hours later transport was evaluated by Spinning disk microscopy [Fig. 11]. The transfection was carried out as already described in 3.10 paragraph. Avidin present in the medium at the

moment of transfection could not be removed, for this reason, to overcome a possible delay in the treatment, the concentration of the Biotin was increased in these experiments up to 80 µM. Movies lasted a minimum of one hour considering at least 3 field per condition in each experiment. Acquisitions were composed by 15 seconds of laser activity followed by 25 seconds in the dark. Live cell imaging experiments were independently repeated three times analyzing more than 20 videos. Fig. 11 show captures from one representative video which confirms the delays found with the analysis performed on fixed cells.

While more work is needed to rule out the role of TBC1D22B in anterograde Golgi to plasma membrane trafficking, the results achieved indicate that TBC1D22B controls ER to Golgi transport by inhibiting one or more RAB GTPases.

We made a first attempt to gain insight on the GAP function of TBC1D22B in the ER to Golgi transport by testing the involvement of the RAB GTPases identified in the TBC1D22B proximity interactome in anterograde transport. To this end, we silenced in BT549 cells the following RABs: RAB1B, RAB6A, RAB8A, RAB13, RAB35 and RAB40A. Forty-eight hours later, cells were transiently transfected with the Li-Str_SBP-EGFP-GPI RUSH construct. Co-localization between the GFP fluorescence of the reporter and the Golgi marker GM130 was measured and compared to control cells. No significant differences were revealed in the speed by which the reporter arrived to the Golgi compartment upon knocking down of the various RABs with the exception of RAB1B which displayed a delay in ER to Golgi trafficking similar to the one found in the cells overexpressing TBC1D22B [Fig.12A-D]. Altogether these findings suggest that TBC1D22B participates in anterograde trafficking, possibly by inhibiting the activity of RAB1B in the ER to Golgi transport.

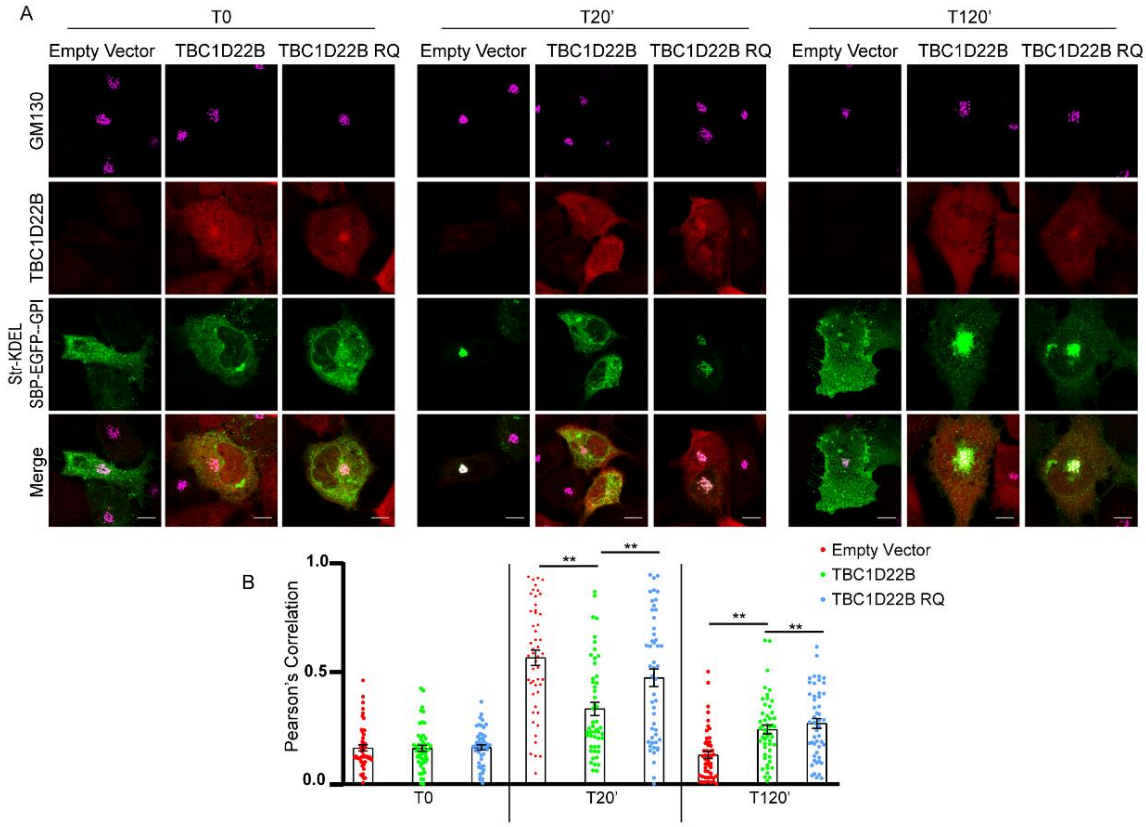

Figure 10. TBC1D22B delays the anterograde pathway.

A) Representative confocal images taken at the time point shown on top, of cells overexpressing the empty vector or TBC1D22B or TBC1D22B RQ (as indicated on top) transiently transfected with the Str-KDEL_SBP-EGFP-GPI construct. Cells were fixed and stained with the antibody against the Golgi marker GM130 (Cell signaling 12480, in magenta) and the anti-TBC1D22B antibody (Novus, H00055633-B01P in red) the GFP fluorescence of the reporter is in green (as indicated on the left). The bar corresponds to 10µm. B) Bar graph showing the extent of colocalization analyzed as the Pearson's Correlation between the GM130 Golgi marker and the RUSH construct at the time points indicated on bottom in the cells as in the legend. Bars are the means ± s.e n=3. **p values<0.005

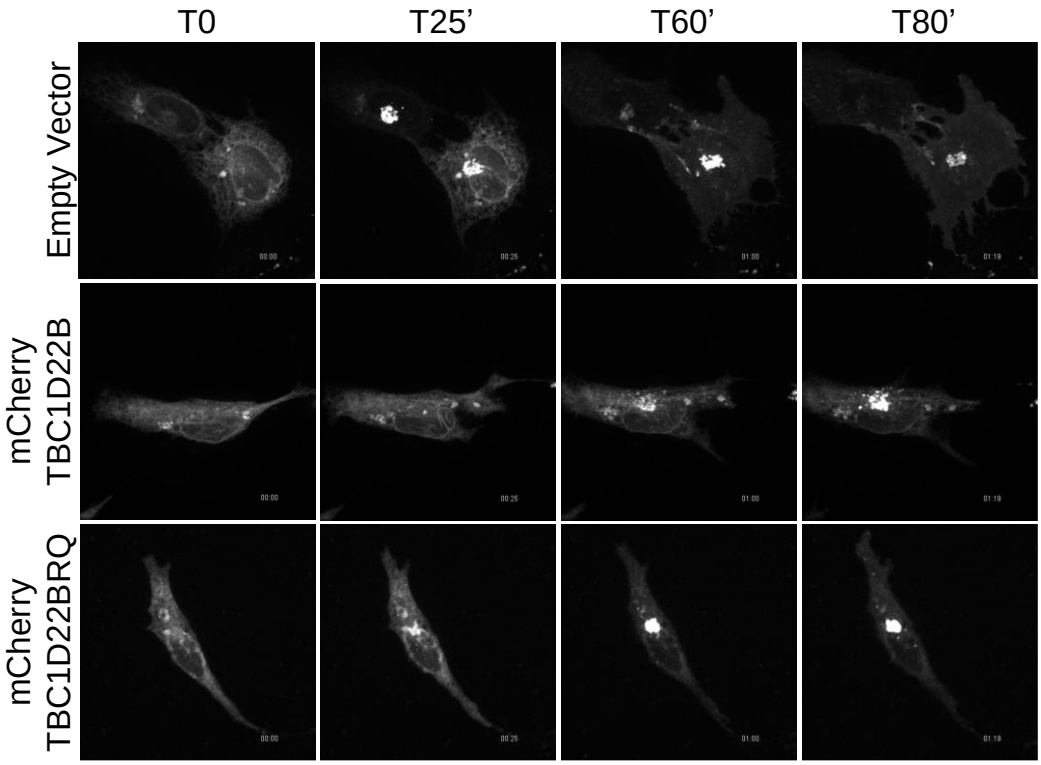

Figure 11. TBC1D22B delays ER to Golgi transport in live cell imaging

BT549 were plated on 25mm coverslips, the day after cells were co-transfected with pRP-mCherry-TBC1D22B or its mutant pRP-mCherry-TBC1D22BRQ together or the empty vector with the Str-KDEL_SBP-EGFP-GPI construct. Live cell imaging was performed using Spinning Disk Microscopy. Snapshots of the time points indicated on top were obtained using ImageJ.

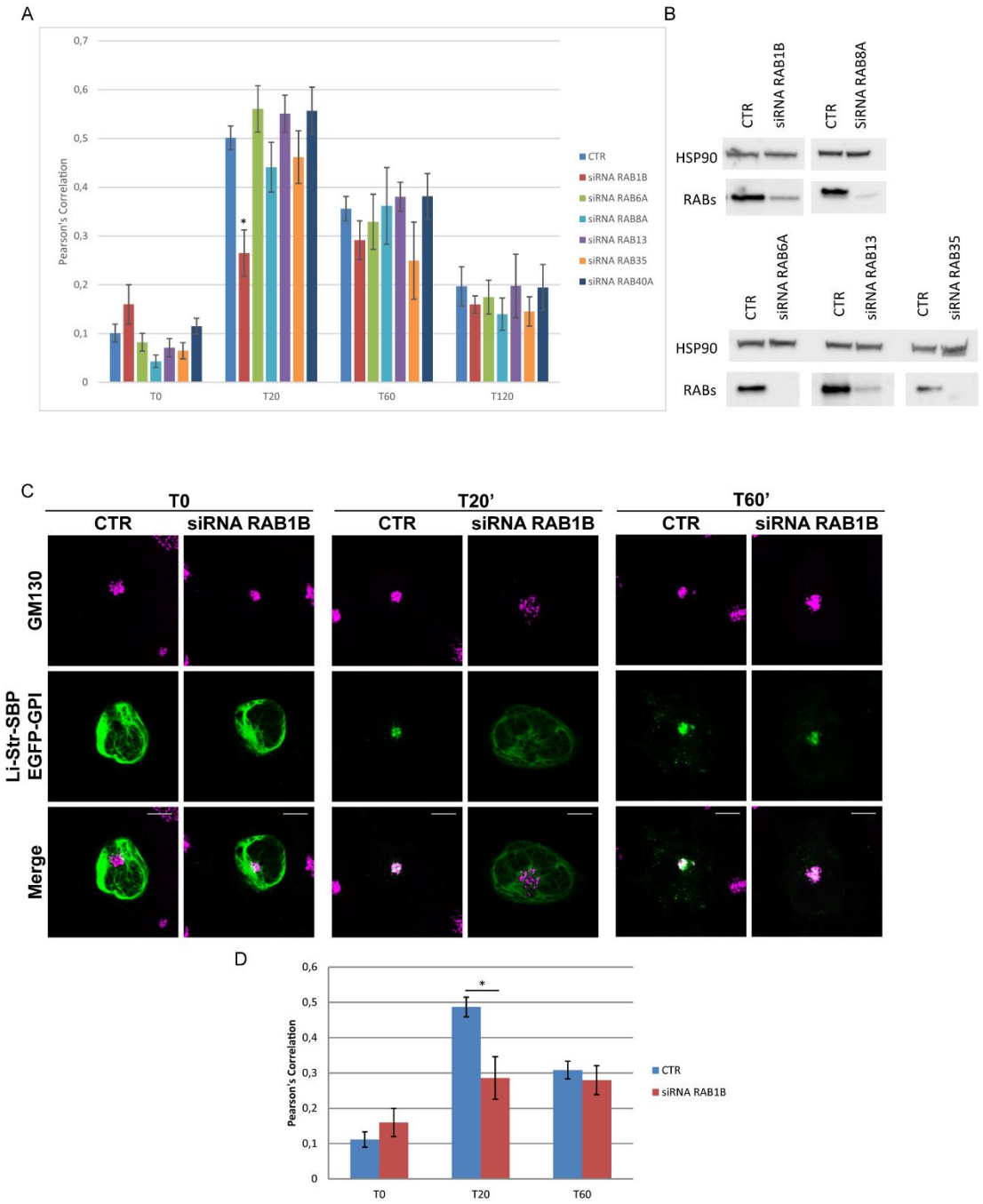

Figure 12. RAB1B silencing affects ER to Golgi transport

A) Bar graph showing the extent of colocalization analyzed as the Pearson's Correlation between the GM130 Golgi marker and the RUSH construct at the time points indicated on bottom in the cells silenced as in the legend. Bars are the means ± s.e n=1. *p values<0.01

B) Total cellular lysates from BT549 cells silenced with CTR siRNA or with pool of four oligoes per each RABs, were immunoblotted as indicated on the left

C) Representative confocal images taken at the time point shown on top, of cells silenced with the non-targeting oligo (CTR) or with the pool of four oligoes per RAB1B (siRNA RAB1B), as indicated on top. After the second day of silencing, cells were transiently transected with the Li-Str-SBP_EGFP-GPI construct. 96h later, cells were fixed and stained with the antibody against the Golgi marker GM130 (Cell signaling 12480, in magenta), the GFP fluorescence of the reporter is in green (as indicated on the left). The bar corresponds to 10µm.
D) Bar graph showing the extent of colocalization analyzed as the Pearson's Correlation between the GM130 Golgi marker and the RUSH construct at the time points indicated on bottom in the cells as in the legend. Bars are the means ± s.e n=2. *p values<0.01

6. Discussion

Breast cancer is a highly aggressive and heterogenous disease. Specific molecular features enable scientist to divide breast cancer patients among the four existing subtypes: Luminal A, Luminal B, HER2+ and Basal like. The first class, Luminal A are characterized by low grade compared to Luminal B which present higher proliferation rate thus, in general, Luminal A have better prognosis. The HER2 overexpressing class include more aggressive malignancies such as grade III tumors with high risk of relapse [1]. Finally, basal like subtype includes the TNBCs which are aggressive cancers showing grater size, lymph node involvement and worst prognosis with higher possibility of relapse within 5 years [1][2]. One of the major limitations in finding new treatments for TNBCs is the lack of common major targets. In the attempt to overcome this limitation, gene expression profiles have been identified from a large cohort of TNBCs identifying seven distinct subclasses: basal-like 1 and 2 (BL1, BL2); immunomodulatory (IM); mesenchymal (M); mesenchymal stem–like (MSL); luminal androgen receptor (LAR); and unstable (UNS) [5]. Subsequent studies have reduced these classes to four: BL1, BL2, LAR and mesenchymal [6]. Moreover, extensive gene expression, gene copy number and mutational status of these tumors have been carried out through the years taking advantage of large datasets such as the METABRIC and the TCGA [9].

In spite of the heterogeneity typical of breast cancers, a common aspect is shared by all the aggressive form of tumors which is the reprogramming of cell metabolism, mostly related to increased glycolysis and lipid metabolism [11]–[14].

Elevation of glycolysis is a major feature of metabolic reprogramming in cancer cells [15]. Increased glycolysis generates metabolites that can be used as building blocks by other metabolic routes to synthetize nucleotide, amino acids and fatty acids required by the rapidly dividing cells to generate the tumour mass [94].

Increased glucose uptake, to feed cancer glycolysis, is exploited in the clinical imaging of tumours through PET which uses the glucose analogue

tracer "2-[^{18}F] fluoro-2-deoxy-D-glucose" (FDG). Avid FDG uptake by cancer cells enables imaging of primary tumours and metastasis with a limit of resolution of around 3-5 mm [95].

Remarkably, high FDG-PET uptake has been recently proposed as a predictor of recurrence in ER-positive BC patients and of response to target therapy at early time points in different tumour types [96]–[99]. Furthermore, a large fraction of TNBCs is characterized by elevated FDG uptake [100] and, at least in pre-clinical models, they seem to depend on this metabolic adaptation for growth and survival [13].

The identification of markers of increased glycolysis in these types of cancers could be exploited as a novel stratification tool. This hypothesis prompted us to search for glycolysis "markers" in breast cancer. We choose to focus on membrane trafficking proteins based on the notion that a key mechanism to elevate glycolysis in cancer cells is to increase or stabilize glucose transporters to the plasma membrane, a process that relies on membrane trafficking [32]. This is commonly achieved by hypoxia and oncogenic lesions such as activation of the EGFR/PI3K/AKT pathway which plays a paramount role in glycolysis elevation [19]. Another common metabolic alteration is the increased lipid metabolism through *de novo* lipogenesis or upregulation of fatty acids internalization from the extracellular environment [14].

Despite the importance of membrane trafficking in sustaining tumours progression, the molecular determinants of signalling-metabolic rewiring in cancer cells are still largely unknown as well as the role of membrane trafficking of nutrient transporters. In the past, our laboratory identified one RabGAP molecule that is amplified in 10% of breast cancers and if responsible of elevated glycolysis mainly in the Basal-like subtype, USP6NL [48]. Mechanistically, we found that high levels of USP6NL delays endocytosis and degradation of the Epidermal Growth Factor Receptor (EGFR) causing chronic AKT activation, which, in turn, stabilizes the glucose transporter GLUT1 to the plasma membrane. This results in increased glucose uptake and elevation of glycolysis [48]. USP6NL belongs

to the family of RabGAP protein, also known as TBC-containing proteins because they share a GTPase Activating Protein (GAP) domain, named the TBC domain [37]. These proteins control the intracellular vesicular trafficking and are involved, at various levels, in the regulation of signal propagation and in the uptake of nutrients, including glucose [32]. While functional ablation of RAB GTPases may cause profound alterations on membrane trafficking as, for instance, depletion of RAB5 impairs the biogenesis of the entire endo-lysosomal system [101], depletion of the RabGAPs seems to have a more restricted impact. Based on this background, we choose to investigate their involvement in glycolysis in breast cancer cells correlating this function with possible alteration in breast tumours. This would allow us to propose them as novel markers of glycolysis elevation in breast cancer.

To address the function of the RabGAPs in glycolysis, we tested the effects of their silencing in high throughput screenings in which we individually silenced each member of the RabGAP family in breast cancer cell measuring the levels of intracellular L-lactate a read out of glycolysis. These screenings allowed us to identified several RabGAPs whose ablation reduces lactate concentration more than 30% compared to control levels, suggesting that these RabGAPs are required for glycolysis. We crossed this information with the analyses done on alteration of RabGAP genes and correlation with breast cancer patient survival to select those RabGAPs that likely participate to breast cancer aggressiveness by increasing tumour metabolic plasticity.

To this end we employed the METABRIC cohort which collects data on gene expression from approximately 2000 breast cancer patients with a long-term clinical follow-up [9] [10]. We found that increased expression of the RabGAPs, TBC1D31, USP6NL, TBC1D7 and TBC1D22B inversely correlates with overall survival in univariate and multivariate analysis in the METABRIC dataset. We extended this analysis, investigating the correlation between survival and mRNA expression/gene copy number, within the breast cancer subtypes, in the METABRIC dataset finding that

USP6NL and TBC1D7 are highly expressed mostly in the TNBC subtype, while TBC1D22B is enriched in the Luminal subtype. By combining the prognostic value of the RabGAPs with the results of the metabolic screenings, we found that four of the six RabGAPs that predict worse patient survival (TBC1D7, TBC1D22B, TBC1D31 and USP6NL) participate in the elevation of glycolysis, arguing that high glycolysis is a prognostic factor in breast cancer.

In search for the role of these molecule in breast cancer metabolic reprogramming, we choose to focus on TBC1D22B because, together USP6NL whose role in glycolysis has been previously depicted, it carries a functional GAP domain, while both TBC1D7 and TBC1D31 do not.

Few information is available on TBC1D22B. In humans, two isoforms exist encoded by distinct genes: TBC1D22A and TBC1D22B. They localize to the Golgi (unpublished observation) and their overexpression has been shown to induce Golgi fragmentation in a GAP-dependent manner [55]. This effect appears to be cell-context dependent since it is evident in HeLa cells but not in telomerase-immortalized human retinal epithelial (hTERT-RPE1) cells [55]. Furthermore, high levels of TBC1D22B disrupt the ERGIC (ER Golgi intermediate compartment) to a greater extent compared to TBC1D22A suggesting distinct functions for these two RabGAPs in the regulation of Golgi morphology [55]. Moreover, recent data showing that TBC1D22A, but not TBC1D22B, inhibits the anterograde transport of G Protein Coupled Receptors (GPCRs) from the ER to the Golgi, further support a non-redundant function of the two isoforms [71].

Both TBC1D22B and TBC1D22A bind to the Golgi resident protein Acyl-CoA binding domain containing 3 (ACBD3) which works as scaffold forming a large multiprotein complex that contains Golgin45, GRASP55 and TBC1D22 at the medial Golgi [67] [102]. Interestingly, GRASP55 has a key role in Golgi cisternae stacking and in unconventional protein secretion of transmembrane receptors from the ER directly to the plasma membrane [103]–[106].

In the attempt to understand the role of TBC1D22B in breast cancer metabolism, first we tested the glycolytic activity and mitochondrial respiration upon TBC1D22B reduction, using the Seahorse technology, finding that they are both reduced. These data suggest that TBC1D22B might have a general function in sustaining the cell energy metabolism or that it controls basic cellular processes whose alteration, in turn, affects cell metabolism. Looking more into the effect of TBC1D22B on nutrient uptake and utilization, we realized that its overexpression promotes the accumulation of lipid droplets. Lipid droplets were found to be increased up to 10 times in cells expressing high levels of the wild type version of TBC1D22B but not the mutated one, indicating a GAP-dependent role for TBC1D22B in lipid metabolism. While the involvement on TBC1D22B in lipid metabolism regulation is not yet understood; it is tempting to speculate regarding the role of this RabGAP protein in lipid storage.

I) TBC1D22B might be involved in *de novo* lipogenesis through the enhancement of reductive glutamine metabolism, thus increasing intracellular fatty acid, hence lipid droplets size within the cell [91].

II) TBC1D22B might increase lipid droplets storage by impairing fatty acid consumption. Upon starvation, LDs are consumed within various processes such as lipophagy to provide fatty acids to mitochondria for beta oxidation. The role of the RabGAP proteins in autophagy has been addressed by Sharon Tooze in a study that highlights the strong inhibitory effect of TBC1D15 on LC3 lipidation upon overexpression [46]. Since TBC1D15 is among the proximity interactors of TBC1D22B, one hypothesis is that overexpression of TBC1D22B promotes lipophagy inhibition indirectly by re-locating or activating another RabGAP molecule.

Of course, further analysis will be required to better understand to specify if TBC1D22B plays a role in increasing lipogenesis rather than reducing lipophagy/ lipolysis.

The involvement of TBC1D22 in lipid metabolism has also been found in the Drosophila model [72]. In Drosophila, there is only one gene, *dTBC1D22,* that is the ortholog of *TBC1D22A* and *TBC1D22B* with *TBC1D22B* showing the highest identity (47%) and similarity (63%) to *dTBC1D22* [72]. Truncating mutation of *dTBC1D22* have been shown to increase the formation of lipid droplets in glia cells and photoreceptor cells of the Drosophila eye. Similarly, simultaneous silencing of the human orthologues TBC1D22A and TBC1D22B in HeLa cells diminished the size of lipid droplets. Our findings showing that overexpression of TBC1D22B in human breast cancer cells induces the accumulation of lipid droplets are not consistent with these results leading to the hypothesis that the role of TBC1D22B in lipid metabolism might be cell-context dependent. In the study on dTBC1D22, colocalization between this RabGAP and the constitutive active mutant of RAB40 is reported as also binding between the overexpressed RAB40 and dTBC1D22BRQ mutant. Moreover, dTBC1D22 can stimulate GTP hydrolysis on RAB40 indicating that, at least in Drosophila, RAB40 is the dTBC1D22B target. Accordingly, the constitutive active RAB40 mutant accumulates lipid droplets similarly to the depletion of its GAP [72]. However, it should be pointed out that the GAP activity of dTBC1D22 on RAB40 has been measured using the immunoprecipitation of dTBC1D22 from Drosophila S2 cells as the source of the RabGAP to be used in the assay. As we will discuss later, this might not be appropriate because the RabGAP proteins are known to interact with each other forming a complex network that coordinate distinct steps of membrane trafficking. Therefore, it is likely (see also our discussion on the results generated on the TBC1D22B proximity interactome) that other RabGAPs are also present in the dTBC1D22B immunoprecipitates and they might be responsible for the hydrolysis of GTP on RAB40.

To avoid similar problems, as we will report later in this discussion, we employed only the recombinant pure TBC1D22B protein and its GAP-defective RQ mutant in our GAP assays.

To understand the role of TBC1D22B in the regulation of cell metabolism, we decided to first identify its protein interacting network and next to address its function in membrane trafficking. Because TBC1D22B is an active enzyme, to identify its interactome, we choose to adopt the proximity biotinylation technique, a method that can intercepts very transient protein-protein interactions such as those occurring during the enzymatic catalysis. While this technique is very powerful, it has a major limitation in the level of specificity of the putative interactions that are found. Indeed, the APEX2 chimera can biotinylate proteins that are not true interactors if it is overexpressed in the cell at location where it should not be usually found. To overcome this problem different approaches can be undertaken. One is to express the chimera in a knockout background, i.e. in a cell that lacks the endogenous protein, or to engineer the chimera using the CRISPR knock-in technique inserting the APEX2 domain in the gene locus that encodes the protein under analysis to express the chimera at endogenous levels. However, even in this case, non-specific biotinylation of proteins can occur for instance during protein synthesis in the ribosome. In the attempt to increase the stringency of our method, we tested different condition of biotinylation playing with both biotin and H_2O_2 concentration. The major improvement that we made to the protocol was to add denaturing agents already in the lysis buffer. This greatly cleaned the controls, strongly reducing the amount of proteins in the pull down from cells expressing the empty vector or APEX2-TBC1D22B but treated with H_2O_2 only. Among the proteins that are part of the APEX2-TBC1D22B proximity interactome we found ABCD3, indicating that, by employing this technique, we were able to detect previously identified physical interactions. Notably, ACBD3 is overexpressed in breast cancer correlating with worse prognosis in multivariate analysis. Mechanistically, ACBD3 appears to promote breast cancer cell self-renewal by activating the Wnt/bactenin signalling pathway [69].

Looking at the protein networks in the TBC1D22B proximity interactome we realized that they were significantly enriched for focal adhesion and cell-cell

junction components in addition to proteins belonging to Golgi vesicles and endoplasmic reticulum exit sites. When we compared the TBC1D22B interactome to the one associated with the GAP defective mutant, we noticed that many focal adhesion and junctional proteins were present in both, however the extracellular matrix receptor integrins ITGA2 and ITGA3 were found to be associated only with the wild type form of the protein, suggesting that integrins trafficking from the ER to the Golgi might be under the control of the TBC1D22B GAP activity. Intriguingly, molecules that are part of the Golgi vesicle transport system, were found preferentially associated with TBC1D22B RQ interactome further suggesting that it might work as a dominant negative mutant in Golgi transport.

Next, we looked for RAB GTPases in the TBC1D22B interactome. The RAB target of TBC1D22B is unknown. We have to mention that TBC1D22A and B are frequently cited as being GAPs for RAB33. However, as far as we know, there are no experimental evidence published in support of this claim. Several RabGTPases were found in the TBC1D22B interactome: RAB1B, RAB6A, RAB7A, RAB8A, RAB13 and RAB35. We hypothesize that at least some of them might not be direct target of the TBC1D22B GAP activity, rather TBC1D22B might be one of their downstream effectors. Interestingly, we noticed other RabGAP proteins are present in the TBC1D22B interactome: RabGAP1 (also named GAPCenA), which was initially identified a GAP for RAB6, and TBC1D15 which is a GAP for RAB7. These two RABs might, therefore, be present in the TBC1D22B interactome because TBC1D22B binds to their negative regulators RabGAP1 and TBC1D15, which in turn bind to their RAB target, generating a network of proteins that is revealed by proximity biotinylation.

Of note, when we compared the interactomes generated by TBC1D22B and its RQ mutant, we did not find any RAB GTPase specifically enriched in the network generated by the enzymatically active wild type form of TBC1D22B. In our opinion, this might be due to the fact that both the two version of TBC1D22B, the wild type molecule and the enzymatically dead version localize to the same membrane microdomain where they can similarly

encounter the RAB GTPase in an environment close enough to allow for the biotinylation by their respective APEX2-chimeras. Alternatively, binding site for these RABs might be present in TBC1D22B outside the GAP domain. Finally, a third, despite questionable, explanation is that mutation of the catalytic residues R and Q would not be sufficient to abrogate the interaction between the GAP and the GTPase.

Whatever the case, we could not exploit the RQ proximity interactome to define which RAB might be the TBC1D22B target. We, therefore, decide to test the GAP activity of purified full length TBC1D22B against the four RABs that were more significantly associated with the TBC1D22B interactome: RAB1B, RAB6A, RAB13 and RAB35 employing the Malachite green phosphate assay using a large excess of the GTP-loaded RAB and catalytic amounts of TBC1D22B (ratio 20:1). TBC1D22B was found to stimulate GTP hydrolysis on all the RABs tested. To confirm the specificity of GTP release measured in our assays, the same GAP assay experiment was repeated using the best performing RAB, RAB1B, in presence of both TBC1D22B and the GAP defective mutant TBC1D22B RQ. The TBC1D22BRQ performed as the negative control (corresponding to the RAB incubated in presence of buffer only) enabling us to conclude that TBC1D22B acts as a GAP for RAB1B *in vitro*.

In the TBC1D22B interactome proteins that control the anterograde ER to Golgi transport as well as the retrograde pathway, including respectively RAB1B and RAB6A, were significantly enriched. These findings, together with the localization of TBC1D22B to the Golgi and the know role of TBC1D22A in ER to Golgi traffic, prompted us to investigate the involvement of TBC1D22B in the anterograde trafficking pathway using the RUSH system. TBC1D22B was found to delay transport from the ER to the Golgi, in a GAP dependent manner. In addition, both the wild type and the mutant delayed transport from the Golgi to the plasma membrane. These data suggest that TBC1D22B controls different steps of the anterograde pathway acting on different RABs both in as a negative regulator (GAP-dependent mechanism) and as an effector (GAP-independent mechanism).

Alternatively, the delay caused by TBC1D22B in Golgi to plasma membrane delivery might result from slowing down the previous step, i.e. the transport from the ER to the Golgi. To gain insights on the mechanism, we focused on disclosing the TBC1D22B RAB target(s) in the regulation of ER to Golgi transport. To this end, we investigated the ER to Golgi transport using the RUSH system in cells that were knocked down for the six RABs that were identified in the TBC1D22B proximity interactome. In agreement with previously published data, only RAB1B was found to delay the ER to Golgi transport similarly to the overexpression of TBC1D22B, further enforcing the notion that RAB1B is a likely target of the TBC1D22B GAP activity both in vitro and in living cells.

Summary and Conclusions

The study performed during this PhD project was aimed to identify novel molecular determinant of glycolysis elevation endowed with prognostic value within the RabGAP family of membrane trafficking proteins.

By combining metabolic screenings and analysis of the correlation between gene expression and survival in breast cancer patients, we identified four RabGAP molecules that participate to glycolysis elevation and predict prognosis in multivariate analysis.

We choose to focus on one of them, TBC1D22B, trying to define its biological function and the mechanism of action. To this end, we identified its interactome finding that it is highly enriched in proteins that control cell adhesion and transport from the ER to the Golgi and plasma membrane suggesting that TBC1D22B plays a role in the delivery of extracellular matrix receptors and focal adhesion components to cell adhesive sites. Using the RUSH system, we, indeed, demonstrate that TBC1D22B restrains the anterograde transport pathway from the ER to the Golgi likely by inhibiting the activity of RAB1B.

How these findings help us to explain the role of TBC1D22B in cell metabolism?

Concerning the function of this RabGAP in metabolic adaptation of breast cancer cells, we found that it is required for the cell energy metabolism and promotes lipid storage. How these effects are related to its role in Golgi trafficking still need to be investigated.

7. Acknowledgement

My gratitude goes to my supervisor Letizia Lanzetti with whom I've been working for the last five years, for creating a stimulating environment at work and pushing me to be better every day. Without her I wouldn't be here. I would like to thank my supervisor Federico Bussolino for believing in this project. Never the less, I would also like to thank my past and present lab members Mariadomenica Lupi, Daniele Avanzato and Rossella Pennisi, for sharing winning and failures with me during these three years of PhD.

8. Bibliography

[1] G. Curigliano *et al.*, “De-escalating and escalating treatments for early-stage breast cancer: The St. Gallen International Expert Consensus Conference on the Primary Therapy of Early Breast Cancer 2017,” *Annals of Oncology*, vol. 28, no. 8, pp. 1700–1712, Aug. 2017, doi: 10.1093/annonc/mdx308.

[2] W. D. Foulkes, I. E. Smith, and J. S. Reis-Filho, “Triple-Negative Breast Cancer,” N Eng. J 2010 Nov 11;363(20):1936-48 doi: 10.1056/NEJMra1001389

[3] I. Januškevičienė and V. Petrikaitė, “Heterogeneity of breast cancer: The importance of interaction between different tumor cell populations,” *Life Sciences*, vol. 239. Elsevier Inc., Dec. 15, 2019. doi: 10.1016/j.lfs.2019.117009.

[4] R. Dent *et al.*, “Triple-negative breast cancer: Clinical features and patterns of recurrence,” *Clinical Cancer Research*, vol. 13, no. 15, pp. 4429–4434, Aug. 2007, doi: 10.1158/1078-0432.CCR-06-3045.

[5] B. D. Lehmann *et al.*, “Identification of human triple-negative breast cancer subtypes and preclinical models for selection of targeted therapies,” *Journal of Clinical Investigation*, vol. 121, no. 7, pp. 2750–2767, Jul. 2011, doi: 10.1172/JCI45014.

[6] B. D. Lehmann *et al.*, “Refinement of triple-negative breast cancer molecular subtypes: Implications for neoadjuvant chemotherapy selection,” *PLoS One*, vol. 11, no. 6, Jun. 2016, doi: 10.1371/journal.pone.0157368.

[7] T. Gruosso *et al.*, “Spatially distinct tumor immune microenvironments stratify triple-negative breast cancers,” *Journal of Clinical Investigation*, vol. 129, no. 4, pp. 1785–1800, 2019, doi: 10.1172/JCI96313.

[8] C. Sotiriou and L. Pusztai, “Gene-Expression Signatures in Breast Cancer,” 2009. N Engl J Med Feb 19;360(8):790-800. Doi:10.1056(NEJMra0801289.

[9] C. Curtis *et al.*, “The genomic and transcriptomic architecture of 2,000 breast tumours reveals novel subgroups,” *Nature*, vol. 486, no. 7403, pp. 346–352, Jun. 2012, doi: 10.1038/nature10983.

[10] G. Ciriello *et al.*, “Comprehensive Molecular Portraits of Invasive Lobular Breast Cancer,” *Cell*, vol. 163, no. 2, pp. 506–519, Oct. 2015, doi: 10.1016/j.cell.2015.09.033.

[11] S. O. Lim *et al.*, “EGFR signaling enhances aerobic glycolysis in triple-negative breast cancer cells to promote tumor growth and immune escape,” *Cancer Res*, vol. 76, no. 5, pp. 1284–1296, Mar. 2016, doi: 10.1158/0008-5472.CAN-15-2478.

[12] D. Groheux *et al.*, “Correlation of high 18F-FDG uptake to clinical, pathological and biological prognostic factors in breast cancer,” *Eur J Nucl Med Mol Imaging*, vol. 38, no. 3, pp. 426–435, Mar. 2011, doi: 10.1007/s00259-010-1640-9.

[13] N. Palaskas *et al.*, “18F-fluorodeoxy-glucose positron emission tomography marks MYC-overexpressing human basal-like breast cancers,” *Cancer Res*, vol. 71, no. 15, pp. 5164–5174, Aug. 2011, doi: 10.1158/0008-5472.CAN-10-4633.

[14] N. Koundouros and G. Poulogiannis, “Reprogramming of fatty acid metabolism in cancer,” *British Journal of Cancer*, vol. 122, no. 1. Springer Nature, pp. 4–22, Jan. 07, 2020. doi: 10.1038/s41416-019-0650-z.

[15] R. J. De Berardinis and N. S. Chandel, “Fundamentals of cancer metabolism,” *Science Advances*, vol. 2, no. 5. American Association for the Advancement of Science, May 01, 2016. doi: 10.1126/sciadv.1600200.

[16] R. J. DeBerardinis and N. S. Chandel, “We need to talk about the Warburg effect,” *Nature Metabolism*, vol. 2, no. 2. Nature Research, pp. 127–129, Feb. 01, 2020. doi: 10.1038/s42255-020-0172-2.

[17] G. Claps *et al.*, “The multiple roles of LDH in cancer,” *Nature Reviews Clinical Oncology*, vol. 19, no. 12. Springer Nature, pp. 749–762, Dec. 01, 2022. doi: 10.1038/s41571-022-00686-2.

[18] S. Dhup, R. K. Dadhich, P. E. Porporato, and P. Sonveaux, “Multiple Biological Activities of Lactic Acid in Cancer: Influences on Tumor Growth, Angiogenesis and Metastasis,” 2012.

[19] L. Wang, S. Zhang, and X. Wang, “The Metabolic Mechanisms of Breast Cancer Metastasis,” *Frontiers in Oncology*, vol. 10. Frontiers Media S.A., Jan. 07, 2021. doi: 10.3389/fonc.2020.602416.

[20] G. L. Semenza, “Hypoxia-inducible factors: coupling glucose metabolism and redox regulation with induction of the breast cancer stem cell phenotype,” *EMBO J*, vol. 36, no. 3, pp. 252–259, Feb. 2017, doi: 10.15252/embj.201695204.

[21] B.J. Altman et al “From Krebs to clinic: Glutamine metabolism to cancer therapy Nature Reviews Cancer 2016 16 (619-634),” *Nat Rev Cancer* 16, 619–634 (2016). https://doi.org/10.1038/nrc.2016.

[22] E. Dornier *et al.*, “Glutaminolysis drives membrane trafficking to promote invasiveness of breast cancer cells,” *Nat Commun*, vol. 8, no. 1, Dec. 2017, doi: 10.1038/s41467-017-02101-2.

[23] I. Elia *et al.*, “Proline metabolism supports metastasis formation and could be inhibited to selectively target metastasizing cancer cells,” *Nat Commun*, vol. 8, May 2017, doi: 10.1038/ncomms15267.

[24] I. Elia *et al.*, “Breast cancer cells rely on environmental pyruvate to shape the metastatic niche,” *Nature*, vol. 568, no. 7750, pp. 117–121, Apr. 2019, doi: 10.1038/s41586-019-0977-x.

[25] N. N. Pavlova and C. B. Thompson, “The Emerging Hallmarks of Cancer Metabolism,” *Cell Metabolism*, vol. 23, no. 1. Cell Press, pp. 27–47, Jan. 12, 2016. doi: 10.1016/j.cmet.2015.12.006.

[26] M. E. Monaco, “Fatty acid metabolism in breast cancer subtypes,” Oncotarget 2017. 8(17):2948729500. Doi:10.18632/oncotarget.15494.

[27] J. A. Olzmann and P. Carvalho, “Dynamics and functions of lipid droplets,” *Nature Reviews Molecular Cell Biology*, vol. 20, no. 3. Nature Publishing Group, pp. 137–155, Mar. 01, 2019. doi: 10.1038/s41580-018-0085-z.

[28] F. Wilfling, J. T. Haas, T. C. Walther, and R. V. F. Jr, “Lipid droplet biogenesis,” *Current Opinion in Cell Biology*, vol. 29, no. 1. Elsevier Ltd, pp. 39–45, 2014. doi: 10.1016/j.ceb.2014.03.008.

[29] E. Jarc and T. Petan, “Lipid Droplets and the Management of Cellular Stress,” Yale J Biol Med 2019. 20;92(3):435-452.

[30] R. Zechner, F. Madeo, and D. Kratky, “Cytosolic lipolysis and lipophagy: Two sides of the same coin,” *Nature Reviews Molecular Cell Biology*, vol. 18, no. 11. Nature Publishing Group, pp. 671–684, 2017. doi: 10.1038/nrm.2017.76.

[31] S. Sigismund, L. Lanzetti, G. Scita, and P. P. Di Fiore, “Endocytosis in the context-dependent regulation of individual and collective cell properties,” *Nature Reviews Molecular Cell Biology*, vol. 22, no. 9. Nature Research, pp. 625–643, Sep. 01, 2021. doi: 10.1038/s41580-021-00375-5.

[32] Costin N. Antonescu, “The intricate relationship between metabolism and endocyticmembrane traffic,” *Wiley Traffic*, Dec. 2016, doi: 10.1111/tra.12695.

[33] S. Rahmani, M. S. Defferrari, W. W. Wakarchuk, and C. N. Antonescu, “Energetic adaptations: Metabolic control of endocytic

membrane traffic," *Traffic*, vol. 20, no. 12. Blackwell Munksgaard, pp. 912–931, Dec. 01, 2019. doi: 10.1111/tra.12705.

[34] H. Stenmark, "Rab GTPases as coordinators of vesicle traffic," *Nature Reviews Molecular Cell Biology*, vol. 10, no. 8. pp. 513–525, Aug. 2009. doi: 10.1038/nrm2728.

[35] R. Jahn and R. H. Scheller, "SNAREs - Engines for membrane fusion," *Nature Reviews Molecular Cell Biology*, vol. 7, no. 9. pp. 631–643, Sep. 19, 2006. doi: 10.1038/nrm2002.

[36] M. Zerial and H. Mcbride, "RAB PROTEINS AS MEMBRANE ORGANIZERS" Nat Rev Mol Cell Biol 2001. Feb; 2(2):107-17 doi:10.1038(3)5052055

[37] M. Fukuda, "TBC proteins: GAPs for mammalian small GTPase Rab?," *Bioscience Reports*, vol. 31, no. 3. pp. 159–168, Jun. 2011. doi: 10.1042/BSR20100112.

[38] X. Pan, S. Eathiraj, M. Munson, and D. G. Lambright, "TBC-domain GAPs for Rab GTPases accelerate GTP hydrolysis by a dual-finger mechanism," *Nature*, vol. 442, no. 7100, pp. 303–306, Jul. 2006, doi: 10.1038/nature04847.

[39] M. A. M. Frasa, K. T. Koessmeier, M. R. Ahmadian, and V. M. M. Braga, "Illuminating the functional and structural repertoire of human TBC/RABGAPs," *Nat Rev Mol Cell Biol*, vol. 13, no. 2, pp. 67–73, Feb. 2012, doi: 10.1038/nrm3267.

[40] E. Fuchs, A. K. Haas, R. A. Spooner, S. I. Yoshimura, J. M. Lord, and F. A. Barr, "Specific Rab GTPase-activating proteins define the Shiga toxin and epidermal growth factor uptake pathways," *Journal of Cell Biology*, vol. 177, no. 6, pp. 1133–1143, Jun. 2007, doi: 10.1083/jcb.200612068.

[41] R. M. Nottingham, G. V. Pusapati, I. G. Ganley, F. A. Barr, D. G. Lambright, and S. R. Pfeffer, "RUTBC2 protein, a Rab9A effector

and GTPase-activating protein for Rab36," *Journal of Biological Chemistry*, vol. 287, no. 27, pp. 22740–22748, Jun. 2012, doi: 10.1074/jbc.M112.362558.

[42] A. F. A. Henriques *et al.*, "WNK1 phosphorylation sites in TBC1D1 and TBC1D4 modulate cell surface expression of GLUT1," *Arch Biochem Biophys*, vol. 679, Jan. 2020, doi: 10.1016/j.abb.2019.108223.

[43] E. Frittoli *et al.*, "The Primate-specific Protein TBC1D3 Is Required for Optimal Macropinocytosis in a Novel ARF6-dependent Pathway," *Mol Biol Cell*, vol. 19, pp. 1304–1316, 2008, doi: 10.1091/mbc.E07-06.

[44] L. Lanzetti, "Rab5 is a signalling GTPases," *Nature*, vol. 429, 2004. 429(6989):309-314 doi:10.1038/nature02542 PMID:15152255

[45] D. J. Sidjanin, A. K. Park, A. Ronchetti, J. Martins, and W. T. Jackson, "TBC1D20 mediates autophagy as a key regulator of autophagosome maturation," *Autophagy*, vol. 12, no. 10, pp. 1759–1775, Oct. 2016, doi: 10.1080/15548627.2016.1199300.

[46] A. Longatti, C. A. Lamb, M. Razi, S. I. Yoshimura, F. A. Barr, and S. A. Tooze, "TBC1D14 regulates autophagosome formation via Rab11- and ULK1-positive recycling endosomes," *Journal of Cell Biology*, vol. 197, no. 5, pp. 659–675, May 2012, doi: 10.1083/jcb.201111079.

[47] D. Popovic, M. Akutsu, I. Novak, J. W. Harper, C. Behrends, and I. Dikic, "Rab GTPase-Activating Proteins in Autophagy: Regulation of Endocytic and Autophagy Pathways by Direct Binding to Human ATG8 Modifiers," *Mol Cell Biol*, vol. 32, no. 9, pp. 1733–1744, May 2012, doi: 10.1128/mcb.06717-11.

[48] D. Avanzato *et al.*, "High USP6NL levels in breast cancer sustain chronic AKT phosphorylation and GLUT1 stability fueling aerobic

glycolysis," *Cancer Res*, vol. 78, no. 13, pp. 3432–3444, Jul. 2018, doi: 10.1158/0008-5472.CAN-17-3018.

[49] B. Goud, S. Liu, and B. Storrie, "Rab proteins as major determinants of the Golgi complex structure," *Small GTPases*, vol. 9, no. 1–2, pp. 66–75, Mar. 2018, doi: 10.1080/21541248.2017.1384087.

[50] R. Duden, "ER-to-Golgi transport: COP I and COP II function," *Molecular Membrane Biology*, vol. 20, no. 3. pp. 197–207, Jul. 2003. doi: 10.1080/0968768031000122548.

[51] S. J. Scales and R. Pepperkok, "Visualization of ER-to-Golgi Transport in Living Cells Reveals a Sequential Mode of Action for COPII and COPI," Cell 1997 Sep. 19;90(6):1137-48. Doi:10.1016/s00928674(00)80379-7.

[52] B. Goud and P. A. Gleeson, "TGN golgins, Rabs and cytoskeleton: Regulating the Golgi trafficking highways," *Trends in Cell Biology*, vol. 20, no. 6. pp. 329–336, Jun. 2010. doi: 10.1016/j.tcb.2010.02.006.

[53] B. Goud, S. Liu, and B. Storrie, "Rab proteins as major determinants of the Golgi complex structure," *Small GTPases*, vol. 9, no. 1–2, pp. 66–75, Mar. 2018, doi: 10.1080/21541248.2017.1384087.

[54] T. Weide, M. Bayer, M. Köster, J.-P. Siebrasse, R. Peters, and A. Barnekow, "The Golgi matrix protein GM130: a specific interacting partner of the small GTPase rab1b," EMBO Reports, April 2001. 2(4):336-341 doi:10.1093/emboreports/kve065 PMDI:11306556

[55] A. K. Haas, S. I. Yoshimura, D. J. Stephens, C. Preisinger, E. Fuchs, and F. A. Barr, "Analysis of GTPase-activating proteins: Rab1 and Rab43 are key Rabs required to maintain a functional Golgi complex in human cells," *J Cell Sci*, vol. 120, no. 17, pp. 2997–3010, Sep. 2007, doi: 10.1242/jcs.014225.

[56] H. Plutner *et al.*, “Rablb Regulates Vesicular Transport between the Endoplasmic Reticulum and Successive Golgi Compartments,” J Cell Biol 1991 115(1):31-43. Doi:10.1083/jcb.115.1.31

[57] B. D. M. W. E. B. Bernard B. Allan, “Rabl Recruitment of p115 into a cis-SNARE Complex: Programming Budding COPII Vesicles for Fusion” Science 2000 jul 21;289(5478):444-8 doi:10.1126/science.289.5478.444

[58] G. Galea, M. G. Bexiga, A. Panarella, E. D. O’Neill, and J. C. Simpson, “A high-content screening microscopy approach to dissect the role of Rab proteins in Golgi-to-ER retrograde trafficking,” *J Cell Sci*, vol. 128, no. 13, pp. 2339–2349, 2015, doi: 10.1242/jcs.167973.

[59] H.-L. Jiang *et al.*, “Loss of RAB1B promotes triple-negative breast cancer metastasis by activating TGF-β/SMAD signaling.” Ocotarget 2015 Jun 30; Doi: 6(18): 16352–16365

[60] N. Halberg, C. A. Sengelaub, K. Navrazhina, H. Molina, K. Uryu, and S. F. Tavazoie, “PITPNC1 Recruits RAB1B to the Golgi Network to Drive Malignant Secretion,” *Cancer Cell*, vol. 29, no. 3, pp. 339–353, Mar. 2016, doi: 10.1016/j.ccell.2016.02.013.

[61] J. D. Thomas *et al.*, “Rab1A Is an mTORC1 Activator and a Colorectal Oncogene,” *Cancer Cell*, vol. 26, no. 5, pp. 754–769, Nov. 2014, doi: 10.1016/j.ccell.2014.09.008.

[62] A. Echard *et al.*, “Alternative Splicing of the Human Rab6A Gene Generates Two Close but Functionally Different Isoforms,” Mol Biol Cell 2000 Nov; 11(11):3819-3833. Doi:10.1091/mbc.11.11.3819

[63] M.-H. Hé *et al.*, “Characterization of GAPCenA, a GTPase activating protein for Rab6, part of which associates with the centrosome,” The EMBO Journal 1999. 18:1772-1782 doi: 10.1093/emboj/18.7.1772

[64] G. V. Pusapati, G. Luchetti, and S. R. Pfeffer, “Ric1-Rgp1 complex is a guanine nucleotide exchange factor for the late Golgi Rab6A

GTPase and an effector of the medial Golgi Rab33B GTPase," *Journal of Biological Chemistry*, vol. 287, no. 50, pp. 42129–42137, Dec. 2012, doi: 10.1074/jbc.M112.414565.

[65] L. Fourriere *et al.*, "RAB6 and microtubules restrict protein secretion to focal adhesions," *Journal of Cell Biology*, vol. 218, no. 7, pp. 2215–2231, 2019, doi: 10.1083/jcb.201805002.

[66] S. Miserey-Lenkei *et al.*, "Coupling fission and exit of RAB6 vesicles at Golgi hotspots through kinesin-myosin interactions," *Nat Commun*, vol. 8, no. 1, Dec. 2017, doi: 10.1038/s41467-017-01266-0.

[67] A. L. Greninger, G. M. Knudsen, M. Betegon, A. L. B. Burlingame, and J. L. DeRisi, "ACBD3 interaction with TBC1 domain 22 protein is differentially affected by enteroviral and kobuviral 3A protein binding," *mBio*, vol. 4, no. 2, Mar. 2013, doi: 10.1128/mBio.00098-13.

[68] J. Liao *et al.*, "ACBD3 is required for FAPP2 transferring glucosylceramide through maintaining the Golgi integrity," *J Mol Cell Biol*, vol. 11, no. 2, pp. 107–117, Nov. 2018, doi: 10.1093/jmcb/mjy030.

[69] Y. Huang *et al.*, "Overexpressed ACBD3 has prognostic value in human breast cancer and promotes the self-renewal potential of breast cancer cells by activating the Wnt/beta-catenin signaling pathway," *Exp Cell Res*, vol. 363, no. 1, pp. 39–47, Feb. 2018, doi: 10.1016/j.yexcr.2018.01.003.

[70] K. Motani, N. Saito-Tarashima, K. Nishino, S. Yamauchi, N. Minakawa, and H. Kosako, "The Golgi-resident protein ACBD3 concentrates STING at ER-Golgi contact sites to drive export from the ER," *Cell Rep*, vol. 41, no. 12, Dec. 2022, doi: 10.1016/j.celrep.2022.111868.

[71] Z. Wei *et al.*, “Specific TBC Domain-Containing Proteins Control the ER-Golgi-Plasma Membrane Trafficking of GPCRs,” *Cell Rep*, vol. 28, no. 2, pp. 554-566.e4, Jul. 2019, doi: 10.1016/j.celrep.2019.05.033.

[72] X. Duan *et al.*, “Regulation of lipid homeostasis by the TBC protein dTBC1D22 via modulation of the small GTPase Rab40 to facilitate lipophagy,” *Cell Rep*, vol. 36, no. 9, Aug. 2021, doi: 10.1016/j.celrep.2021.109541.

[73] V. Hung *et al.*, “Spatially resolved proteomic mapping in living cells with the engineered peroxidase APEX2,” *Nat Protoc*, vol. 11, no. 3, pp. 456–475, Mar. 2016, doi: 10.1038/nprot.2016.018.

[74] Y. Han *et al.*, “Directed Evolution of Split APEX2 Peroxidase,” *ACS Chem Biol*, vol. 14, no. 4, pp. 619–635, Apr. 2019, doi: 10.1021/acschembio.8b00919.

[75] B. T. Lobingier *et al.*, “An Approach to Spatiotemporally Resolve Protein Interaction Networks in Living Cells,” *Cell*, vol. 169, no. 2, pp. 350-360.e12, Apr. 2017, doi: 10.1016/j.cell.2017.03.022.

[76] B. Tan, S. Peng, S. M. J. M. Yatim, J. Gunaratne, W. Hunziker, and A. Ludwig, “An Optimized Protocol for Proximity Biotinylation in Confluent Epithelial Cell Cultures Using the Peroxidase APEX2,” *STAR Protoc*, vol. 1, no. 2, Sep. 2020, doi: 10.1016/j.xpro.2020.100074.

[77] K. Bersuker *et al.*, “A Proximity Labeling Strategy Provides Insights into the Composition and Dynamics of Lipid Droplet Proteomes,” *Dev Cell*, vol. 44, no. 1, pp. 97-112.e7, Jan. 2018, doi: 10.1016/j.devcel.2017.11.020.

[78] J. R. Tran *et al.*, “An apex2 proximity ligation method for mapping interactions with the nuclear lamina,” *Journal of Cell Biology*, vol. 220, no. 1, Jan. 2021, doi: 10.1083/jcb.202002129.

[79] H. W. Rhee *et al.*, “Proteomic mapping of mitochondria in living cells via spatially restricted enzymatic tagging,” *Science (1979)*, vol. 339, no. 6125, pp. 1328–1331, Mar. 2013, doi: 10.1126/science.1230593.

[80] F. M. Fazal *et al.*, “Atlas of Subcellular RNA Localization Revealed by APEX-Seq,” *Cell*, vol. 178, no. 2, pp. 473-490.e26, Jul. 2019, doi: 10.1016/j.cell.2019.05.027.

[81] T. Del Olmo *et al.*, “APEX2-mediated RAB proximity labeling identifies a role for RAB21 in clathrin-independent cargo sorting,” *EMBO Rep*, vol. 20, no. 2, Feb. 2019, doi: 10.15252/embr.201847192.

[82] Jianjiong Gao et al, “Integrative Analysis of Complex Cancer Genomics and Clinical Profiles Using the cBioPortal,” vol. 6, no. 269, pp. 1–34, 2014, doi: 10.1126/scisignal.2004088.Integrative.

[83] S. Tyanova, T. Temu, and J. Cox, “The MaxQuant computational platform for mass spectrometry-based shotgun proteomics,” *Nat Protoc*, vol. 11, no. 12, pp. 2301–2319, Dec. 2016, doi: 10.1038/nprot.2016.136.

[84] J. Cox, N. Neuhauser, A. Michalski, R. A. Scheltema, J. V. Olsen, and M. Mann, “Andromeda: A peptide search engine integrated into the MaxQuant environment,” *J Proteome Res*, vol. 10, no. 4, pp. 1794–1805, Apr. 2011, doi: 10.1021/pr101065j.

[85] J. Rgen Cox, M. Y. Hein, C. A. Luber, I. Paron, N. Nagaraj, and M. Mann, “Accurate Proteome-wide Label-free Quantification by Delayed Normalization and Maximal Peptide Ratio Extraction, Termed MaxLFQ* □ S Technological Innovation and Resources,” *Molecular & Cellular Proteomics*, vol. 13, pp. 2513–2526, 2014, doi: 10.1074/mcp.

[86] N. T. Doncheva, J. H. Morris, J. Gorodkin, and L. J. Jensen, “Cytoscape StringApp: Network Analysis and Visualization of Proteomics Data,” *J Proteome Res*, vol. 18, no. 2, pp. 623–632, Feb. 2019, doi: 10.1021/acs.jproteome.8b00702.

[87] G. Boncompain and F. Perez, “Synchronizing protein transport in the secretory pathway,” *Curr Protoc Cell Biol*, no. SUPPL.57, 2012, doi: 10.1002/0471143030.cb1519s57.

[88] B. Pereira *et al.*, “The somatic mutation profiles of 2,433 breast cancers refines their genomic and transcriptomic landscapes,” *Nat Commun*, vol. 7, May 2016, doi: 10.1038/ncomms11479.

[89] H. Pan *et al.*, “20-Year Risks of Breast-Cancer Recurrence after Stopping Endocrine Therapy at 5 Years,” *New England Journal of Medicine*, vol. 377, no. 19, pp. 1836–1846, Nov. 2017, doi: 10.1056/nejmoa1701830.

[90] P. S. Bernard *et al.*, “Supervised risk predictor of breast cancer based on intrinsic subtypes,” *Journal of Clinical Oncology*, vol. 27, no. 8, pp. 1160–1167, Mar. 2009, doi: 10.1200/JCO.2008.18.1370.

[91] R. J. Deberardinis *et al.*, “Beyond aerobic glycolysis: Transformed cells can engage in glutamine metabolism that exceeds the requirement for protein and nucleotide synthesis,” Proc Natl Acad Sci U S A. 2007 Dec 4;104(49):19345-50. doi: 10.1073/pnas.0709747104. Epub 2007 Nov 21. PMID: 18032601; PMCID: PMC2148292.

[92] P. Icard *et al.*, “Understanding the central role of citrate in the metabolism of cancer cells and tumors: An update,” *International Journal of Molecular Sciences*, vol. 22, no. 12. MDPI, Jun. 02, 2021. doi: 10.3390/ijms22126587.

[93] G. Boncompain *et al.*, “Synchronization of secretory protein traffic in populations of cells,” *Nat Methods*, vol. 9, no. 5, pp. 493–498, May 2012, doi: 10.1038/nmeth.1928.

[94] R. A. Gatenby and R. J. Gillies, “Why do cancers have high aerobic glycolysis?,” *Nature Reviews Cancer*, vol. 4, no. 11. pp. 891–899, Nov. 2004. doi: 10.1038/nrc1478.

[95] W. W. Moses, “Fundamental limits of spatial resolution in PET,” *Nucl Instrum Methods Phys Res A*, vol. 648, no. SUPPL. 1, Aug. 2011, doi: 10.1016/j.nima.2010.11.092.

[96] George D Demetri *et al.*, “EFFICACY AND SAFETY OF IMATINIB MESYLATE IN ADVANCED GASTROINTESTINAL STROMAL TUMORS,” N Engl J Med 2002; 347:472-480 DOI: 10.1056/NEJMoa0204612002.

[97] S. Lheureux *et al.*, “18F-FDG is a surrogate marker of therapy response and tumor recovery after drug withdrawal during treatment with a dual PI3K/mTOR inhibitor in a preclinical model of cisplatin-resistant ovarian cancer,” *Transl Oncol*, vol. 6, no. 5, pp. 586–595, 2013, doi: 10.1593/tlo.13100.

[98] L. Nogová *et al.*, “Downregulation of 18F-FDG uptake in PET as an early pharmacodynamic effect in treatment of non-small cell lung cancer with the mTOR inhibitor everolimus,” *Journal of Nuclear Medicine*, vol. 50, no. 11, pp. 1815–1819, Nov. 2009, doi: 10.2967/jnumed.109.065367.

[99] J. Maynard, S. A. Ricketts, C. Gendrin, P. Dudley, and B. R. Davies, “2-Deoxy-2-[18F]fluoro-d-glucose positron emission tomography demonstrates target inhibition with the potential to predict anti-tumour activity following treatment with the AKT inhibitor AZD5363,” *Mol Imaging Biol*, vol. 15, no. 4, pp. 476–485, Aug. 2013, doi: 10.1007/s11307-013-0613-3.

[100] S. Basu *et al.*, “Comparison of triple-negative and estrogen receptor-positive/progesterone receptor-positive/HER2-negative breast carcinoma using quantitative fluorine-18 fluorodeoxyglucose/positron emission tomography imaging parameters: A potentially useful method for disease characterization,” *Cancer*, vol. 112, no. 5, pp. 995–1000, Mar. 2008, doi: 10.1002/cncr.23226.

[101] A. Zeigerer *et al.*, “Rab5 is necessary for the biogenesis of the endolysosomal system in vivo,” *Nature*, vol. 485, no. 7399, pp. 465–470, May 2012, doi: 10.1038/nature11133.

[102] X. Yue *et al.*, “ACBD3 functions as a scaffold to organize the Golgi stacking proteins and a Rab33b-GAP,” *FEBS Lett*, vol. 591, no. 18, pp. 2793–2802, Sep. 2017, doi: 10.1002/1873-3468.12780.

[103] J. Kim *et al.*, “Monomerization and ER Relocalization of GRASP Is a Requisite for Unconventional Secretion of CFTR,” *Traffic*, vol. 17, no. 7, pp. 733–753, Jul. 2016, doi: 10.1111/tra.12403.

[104] H. Y. Gee, J. Kim, and M. G. Lee, “Unconventional secretion of transmembrane proteins,” *Seminars in Cell and Developmental Biology*, vol. 83. Elsevier Ltd, pp. 59–66, Nov. 01, 2018. doi: 10.1016/j.semcdb.2018.03.016.

[105] C. Rabouille, “Pathways of Unconventional Protein Secretion,” *Trends in Cell Biology*, vol. 27, no. 3. Elsevier Ltd, pp. 230–240, Mar. 01, 2017. doi: 10.1016/j.tcb.2016.11.007.

[106] Y. Xiang and Y. Wang, “GRASP55 and GRASP65 play complementary and essential roles in Golgi cisternal stacking,” *Journal of Cell Biology*, vol. 188, no. 2, pp. 237–251, Jan. 2010, doi: 10.1083/jcb.200907132.